POPULAR DEMOCRATIC REPUBLIC OF ALGERIA

MINISTRY OF HIGHER EDUCATION AND SCIENTIFIC RESEARCH

University of Mohamed El-Bachir El-Ibrahimi , Bordj Bou Arreridj

Faculty of *Sciences and Technology*

Electronics departement

Thesis

Presented to obtain

The MASTER's degree in

Electronic industries

by :

- **Souhayb Atir**
- **Islam Laib**

Entitled :

A graded bandgap perovskite solar cell

Defended on : 26 / 06 /2024

Evaluation committee :

Full Name	*Grade*	*Quality*	*Establishment*
Mrs F. Kherrat	*MAA*	*Président*	*Univ-BBA*
Mrs F. Khaled	*MCB*	*Superviser*	*Univ-BBA*
Mrs F. Farès	*MCA*	*Examiner*	*Univ-BBA*

2023/2024

Table of Contents

Chapter 1

chapter 2

Table of contents

chapter 3

Table of contents

List of figures

List of figures

List of tables

Abbreviations and nomenclature

Abbreviations

PV - Photovoltaic

ETL - Electron Transport Layer

HTL - Hole Transport Layer

PCE - Power Conversion Efficiency

IV - Current-Voltage

QE - Quantum Efficiency

EQE - External Quantum Efficiency

IQE - Internal Quantum Efficiency

PSC - Perovskite Solar Cell

MAPb(I1−xBrx)3 - Methylammonium Lead Halide Perovskite

CH3NH3PbX3 - Methylammonium Lead Halide Perovskite (where X can be Iodine, Bromine, or Chlorine)

VOC - Open-Circuit Voltage

FF - Fill Factor

AM1.5 - Air Mass 1.5 (a standard solar spectrum)

Rs - Series Resistance

Rsh - Shunt Resistance

STC - Standard Test Conditions

ITO - Indium Tin Oxide

Spiro-OMeTAD - 2,2',7,7'-Tetrakis(N,N-di-p-methoxyphenylamine)-9,9'-spirobifluorene

TiO2 - Titanium Dioxide

ALD - Atomic Layer Deposition

HBr - Hydrogen Bromide

MABr - Methylammonium Bromide

Abbreviations and nomenclature

PbI2 - Lead Iodide

FTO - Fluorine-doped Tin Oxide

NIR - Near-Infrared

Eg - Bandgap Energy

T - Temperature

q - Elementary Charge of an Electron

I0 - Dark Saturation Current

IL - Photocurrent Generated by Light

Vm - Voltage at Maximum Power Point

Im - Current at Maximum Power Point

Pin - Incident Power

MAPbBr3 - Methylammonium Lead Bromide Perovskite

MAPbI3 - Methylammonium Lead Iodide Perovskite

MAPbI3-xBrx - Methylammonium Lead Mixed Halide Perovskite

SRH - Shockley-Read-Hall

Nomenclature

A - Area

Eg - Bandgap energy

FF - Fill Factor

Jcc - Current density at short circuit

Isc - Short-circuit current

Vco - Voltage at open circuit

χ - electron affinity

μp - Hole mobility

μn - Electron mobility

τn – Electron lifetime

τp - Hole lifetime.

abstract

ملخص

من أجل فهم خصائص الخلايا الشمسية البيروفسكايت بشكل أفضل - وعلى وجه الخصوص، هيكل $MAPb(I_{1-x}Br_x)_3$ تتناول هذه الدراسة التطورات واستراتيجيات التحسين في تكنولوجيا الخلايا الشمسية الكهروضوئية. تستكشف الدراسة هندسة فجوة النطاق المتدرجة في الطبقة الممتصة لتحسين كفاءة التحويل الكهروضوئي (PCE) باستخدام (C-TiO2) كطبقة نقل الكترونات و Spiro-OMeTAD كطبقة نقل الثقوب يعمل هذا العمل على تعديل نسبة اليود إلى البروم بشكل منهجي من أجل زيادة امتصاص الضوء إلى الحد الأقصى وديناميكيات حامل الشحنة وتحقيق مستوى عالٍ من .PCE ويتناول أيضًا كيفية تأثير تغيير سماكة طبقات الامتصاص و نقل الثقوب و نقل الكترونات ومستويات المنشطات على الكفاءة ككل. تم تحديد التكوين الأمثل من خلال التحليل التجريبي وعمليات المحاكاة الشاملة باستخدام Silvaco ATLAS ب 0.6 ميكرومتر لسمك طبقة الامتصاص، و 0.1 ميكرومتر لكل من طبقة نقل الثقوب و طبقة نقل الكترونات ، ومستويات المنشطات 1e17 لكلا الطبقتين، مما يؤدي إلى كفائة بنسبة 22.35%.

abstract

In order to better understand the properties of perovskite solar cells, more especially, $MAPb(I_{1-x}Br_x)_3$ structure. This study examines advancements and optimization strategies in photovoltaic solar cell technology. The study explores graded bandgap engineering in the absorber layer to improve photovoltaic conversion efficiency (PCE) using (C-TiO2) as (ETL) and Spiro-OMeTAD as (HTL). The work systematically modifies the iodine to bromine ratio in order to maximize light absorption and charge carrier dynamics and attain high PCE. It also looks at how changing the absorber, HTL, and ETL layers' thicknesses and doping levels affects efficiency as a whole. An optimal configuration was determined by empirical analysis and extensive simulations using Silvaco ATLAS: 0.6 μm for the absorber layer thickness, 0.1 μm for the HTL and ETL layers, and $1x\ 10^{17}$ doping levels for both layers, yielding a PCE of 22.35%.

Résumé

Afin de mieux comprendre les propriétés des cellules solaires à pérovskite, plus particulièrement la structure $MAPb(I_{1-x}Br_x)_3$, ce travail examine les avancées et les stratégies d'optimisation dans la technologie des cellules solaires photovoltaïques. L'étude explore l'ingénierie de la bande interdite graduée dans la couche absorbante pour améliorer l'efficacité de conversion photovoltaïque (PCE) en utilisant (C-TiO2) comme (ETL) et Spiro-OMeTAD comme (HTL). Le travail modifie systématiquement le rapport iode/brome afin de maximiser l'absorption de la lumière et la dynamique des porteurs de charge et d'atteindre un PCE élevé. Il examine également comment la modification de l'épaisseur et des niveaux de dopage des couches d'absorbeur, de HTL et d'ETL affecte l'efficacité dans son ensemble. Une configuration optimale a été déterminée par une analyse empirique et des simulations approfondies à l'aide de Silvaco ATLAS : 0,6 μm pour l'épaisseur de la couche absorbante, 0,1 μm pour les couches HTL et ETL et des niveaux de dopage de $1x10^{17}$ pour les deux couches, ce qui donne un PCE de 22,35

General introduction

Perovskite solar cells (PSCs) have attracted attention for use as a next-generation solar cell. Inorganic-organic halide PSCs have excellent optoelectronic properties, such as a low recombination rate, long carrier diffusion length, low fabrication cost, simple and fast fabrication process, and controllable bandgap. More efforts have been devoted to the development of such solar cells and have promoted the rapid increase in their efficiency.

The three primary sections of this work are conventional photovoltaic cells, perovskite solar cells, and then the numerical simulation of solar cells with a uniform bandgap in the first time and a graded one after.

In the first chapter, the principles of photovoltaic solar cells, such as the photovoltaic effect and solar cell forms, are introduced. It discusses quantum efficiency, collection probability, and light-generated current physics. The spectrum response of solar cells as well as important performance indicators including the IV curve, fill factor, open-circuit voltage, short-circuit current, and total efficiency are covered in this chapter. It also looks at how resistance elements, temperature, and light intensity affect solar cell performance.

An Overview of Perovskite solar cells is given in chapter two where the $CH_3NH_3PbX_3$ perovskite light absorber is highlighted. It describes the progress made in developing bandgap tuning methods and graded energy band creation to improve efficiency. The chapter also covers advancements in theory and practice for better optimizing these cells.

In chapter 3, computational simulations perovskite solar cells using the Silvaco Tcad simulator are discussed. It discusses the effects of changing geometrical and doping parameters on photovoltaic performance features. Simulations exploring the spectrum response and optimizing a graded energy bandgap are presented, along with the effects of varying doping doses and thicknesses on the cell efficiency. By modifying the iodine to bromine ratio to maximize solar spectrum absorption and enhance charge carrier dynamics, the work seeks to optimize the graded bandgap in perovskite $MAPb(I_{1-x}Br_x)_3$ solar cells, resulting in higher efficiency. This strategy is essential for improving perovskite solar cells' performance at a reasonable cost and may completely change how photovoltaic systems employ them. Our work is ended by a conclusion.

CHAPTER 1

Photovoltaic solar cell

1.1 Introduction

Photovoltaic (PV) solar cells efficiently transform sunlight into electrical energy by harnessing the photovoltaic effect. Photons, which make up sunlight, transfer energy to electrons in semiconductor materials—typically silicon—when they strike the solar cell. Electrons are stimulated by this energy, which leads to the creation of electron-hole pairs. At the p-n junction, the interface between silicon layers doped to have a large concentration of holes (p-type) and electrons (n-type), the pairs are then separated by the internal electric field. Electric current flows when a device is linked to an external circuit because the separation of charges causes electrons to travel toward the n-type layer and holes to migrate toward the p-type layer. The procedure is made easier by the metallic connections at the top and bottom of the cell.

Important elements influencing a solar cell semiconductor efficiency include: the difference in energy levels between the valence band and the conduction band known as bandgap energy (Eg). The wavelength sensitivity of the semiconductor controls its capacity to absorb light and transform it into electrical energy.
The ease with which electrons and holes can move through a semiconductor material which is referred to as carrier mobility.

The carrier lifetime defined by the average amount of time that carriers can move before recombining. Indeed, a longer lifetime increases the likelihood that carriers will reach the cell's electrodes and contribute to the electric current flow.

The quantity of impurities added to a semiconductor material to produce p-type or n-type properties referred to as the doping concentration directly impact both the cell's efficiency and the strength of the electric field at the p-n junction.

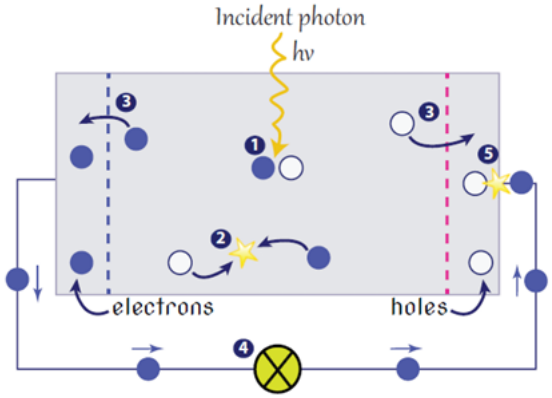

Figure1.1 : Schematic of a very simple solar cell model [1]

1.2 Solar Cell Structure

1.2.1 Light generated current

The term "Light Generated Current" represents the electrical current produced while the cell is exposed to light. Solar cells convert light energy into electricity using the photovoltaic effect. The production of the light-generated current or electric current in a solar cell is based on two basic processes:

When photons with energy higher than the band gap create electron-hole pairs inside the solar cell, photon absorption and electron-hole pair formation occur. These couples are in a state of metastability, which means that they will only last as long as the minority carriers do before reuniting. The electron-hole pair is scattered as a result of recombination, which makes it more difficult to produce current or power.[3]

Carriers aggregating at the p-n junction: The electron and hole are kept apart from recombining by the electric field produced by the p-n junction. When the light-generated minority carrier reaches the p-n junction, it quickly passes through the junction and becomes a majority carrier. An electric current is produced when the solar cell's emitter and base are linked, creating a short circuit. This allows the charge carriers to move across the external circuit.[3]

1.2.2 The collection probability

The collection probability in solar cells is the probability that carriers (electrons and holes) produced by light in the semiconductor will reach the electrodes and contribute to the external current before they combine again.

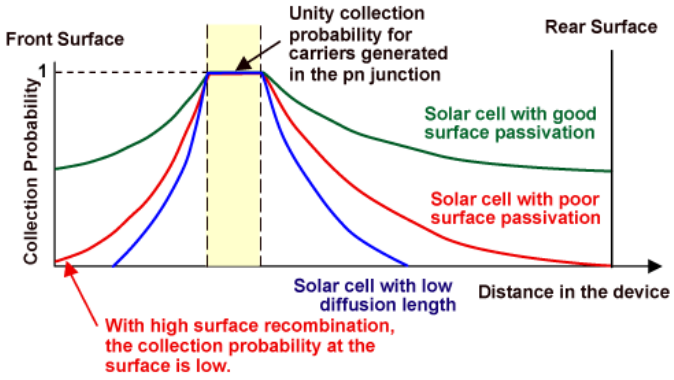

Figure1.2 The spectral response of a silicon solar cell under glass [3]

The equation below governs the collection probability for a device with uniform doping and an abrupt junction

$$\cosh\frac{x}{L}-\frac{\frac{SL}{D}\cosh\frac{W}{L}+\sinh\frac{W}{L}}{\frac{SL}{D}\sinh\frac{W}{L}+\cosh\frac{W}{L}}\sinh\frac{x}{L} \tag{1.1}$$

The above equation simplifies to:

$$CP=\exp\frac{-x}{L} \tag{1.2}$$

1.2.3 Quantum Efficiency

The Quantum Efficiency (QE) of a photovoltaic (PV) cell quantifies the cell's ability to convert incident photons into electrons, which are subsequently utilized to produce an electric current. Here is a comprehensive examination of the components and processes involved in quantitative easing (QE)

1.2.3.1 External Quantum Efficiency (EQE)

This parameter is a measure of the ratio between the number of charge carriers collected by a solar cell and the number of photons that strike it. It encompasses all forms of losses, such as transmission, reflection, and absorption, without considering carrier collection. EQE considers the complete sequence of events starting from the photon's arrival to the charge collection.

The equation for EQE is provided as follows:

$$EQE = \frac{electrons/sec}{photons/sec} = \frac{(current)/(charge\,of\,one\,electron)}{(total\,power\,of\,photons)/(energy\,of\,one\,photon)} \quad (1.3)$$

1.2.3.2 The Internal Quantum Efficiency (IQE)

IQE refers to the proportion of charge carriers that are collected compared to the number of photons that are absorbed by the semiconductor material. In contrast to EQE, IQE disregards losses resulting from reflection or transmission and instead, concentrates entirely on the efficiency of internal processes.

The equation representing the IQE is as follows:

$$IQE = \frac{electrons/sec}{absorbed\,photons/sec} = \frac{EQE}{1-Reflection-Transmission} \quad (1.4)$$

1.2.4 The spectral response

The capacity of a solar cell to effectively transform photons from various light wavelengths into electrical energy is known as its spectral response. It is crucial to comprehend the total effectiveness of solar cells. It indicates how effectively a solar cell can use light from various wavelengths.[22]

1.2.5 The photovoltaic effect

The basic process that makes solar cells function is known as the photovoltaic effect. This phenomenon happens when electromagnetic radiation, such sunlight, strikes two different materials, causing a voltage or potential difference to form at their junction. This has a close relationship to the photoelectric effect, which was explained by Albert Einstein in 1905. He proposed that light is made up of separate particles called photons, each of which has a quantized energy level.

In order to concisely describe the photovoltaic effect in solar cells, three basic mechanisms can be used: Electrons and holes are produced as a result of photon absorption. Electrons are stimulated from the valence band to the conduction band when photons with energy greater than the semiconductor material's bandgap is absorbed. This leads to the production of electron-hole pairs.

Charge carriers are being split up by the electric field such that the holes move toward the p-type side and the electrons toward the n-type side.
Finally, the build-up of charge carriers at the electrodes which results in the production of electricity or a generation of an electrical power.

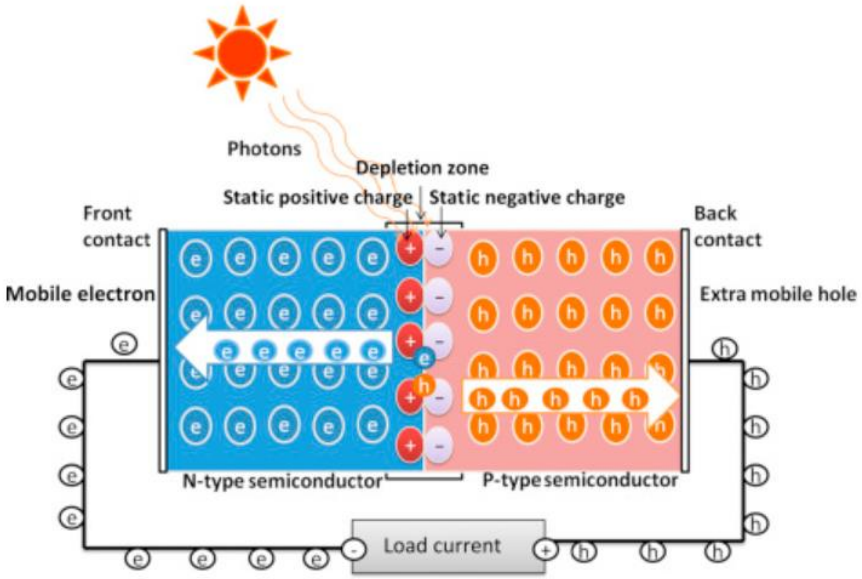

Figure 1.3 : Schematic representation of a simple photovoltaic cell. [2]

1.3 Equivalent circuit

The equivalent circuit of an illuminated PN junction solar cell is shown in Figure 1.4. The PN junction relationship between J and V is represented by equation 1.5.

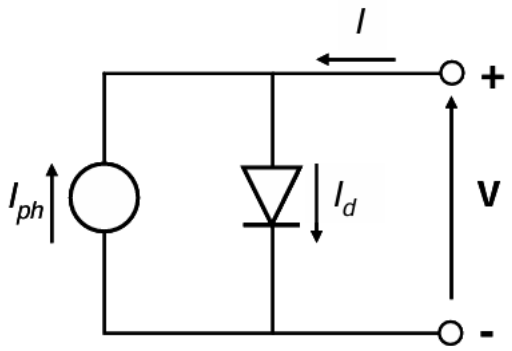

Figure1.4 The equivalent circuit of an ideal solar cell.

$$I = I_0 \left[\exp\left(\frac{qV}{nKT}\right) - 1\right] - I_L \tag{1.5}$$

Where signifies the dark saturation current, q is the elementary charge of an electron, V indicates the voltage across the solar cell, n is the ideality factor, k represents Boltzmann's constant, T is the temperature in Kelvin, and is the photocurrent generated by light. This equation models the solar cell's current-voltage characteristics under illumination. The exponential term depicting the diode's behaviour and countering the forward current as it is produced by the light absorption.

Adding series and shunt resistances to the circuit allows the modelling of the defects present in solar cells.

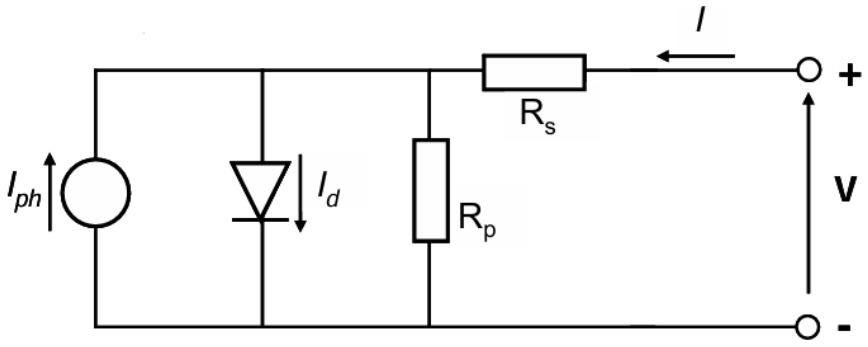

Figure1.5 The equivalent circuit of a solar cell with series and shunt resistance.

$$I = I_0 \left[\exp\left(\frac{q(V - AIR_S)}{KT}\right) - 1\right] + \frac{V - AIR_S}{R_{sh}} - I_L \tag{1.6}$$

The equation (1.6) represents the current-voltage (I-V) characteristics of a real solar cell, where A represents the area of the solar sell

1.4 Solar Cell Parameters

The primary metrics utilized to describe the functionality of solar cells are fill factor (FF), open circuit voltage (Voc), short circuit current (Isc), and peak power (Pmax). As shown in Figure 1.6, these parameters are derived from the lighted I-V characteristic. These characteristics allow for the determination of the conversion efficiency η.

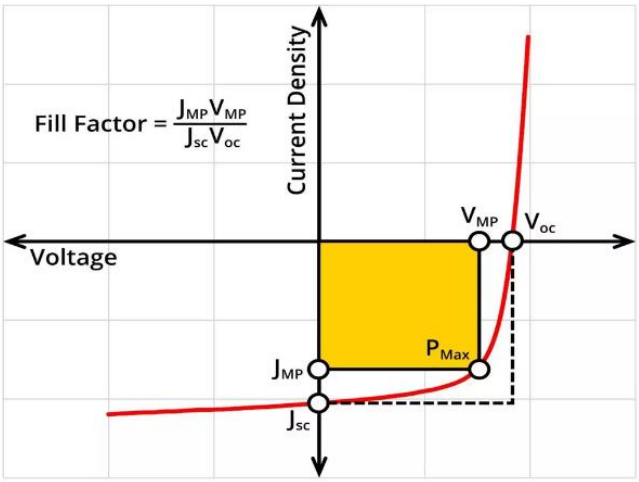

Figure 1.6: J-V characteristics of a p-n junction

1.4.1 The short-circuit current

One of the most important metrics for determining a solar cell's efficiency is its short-circuit current (I_{sc}). The maximum electric current that a solar cell may produce when its terminals are directly connected to each other in the absence of an external load is known as the short-circuit current. This condition occurs, when there is no voltage across the solar cell. The short-circuit current (I_{sc}) is the point on the solar cell's current-voltage (IV) curve where the voltage (V) is zero. [5]

1.4.2 Open-circuit voltage (V_{OC}):

The open-circuit voltage (V_{OC}) is a critical parameter that provides important insights into the device's potential efficiency. The maximum voltage a solar cell can produce when it is

disconnected from all external loads and there is no current passing through it is known as open-circuit voltage. This voltage is referred to as V_{OC}. [5]

$$V_{oc} = \frac{nKT}{q} \ln\left(\frac{I_L}{I_0} + 1\right) \quad (1.7)$$

1.4.3 Fill Factor

An essential metric for assessing a solar cell's performance and efficiency is its Fill Factor (FF). It gives an indication of how well a solar cell converts sunlight into electrical energy. The current-voltage (IV) curve of a solar cell's rectangular shape is quantified by the Fill Factor. It shows the ratio of the theoretical power output that would result from concurrently reaching the maximum values of voltage and current to the highest achievable power output. When operating under conditions that yield the greatest output power, voltage V_m, and current I_m at the optimal operating point, the solar cell's fill factor (FF) is displayed in Figure 1.12. The formula of the FF is defined by the following expression:

$$FF = \frac{V_m I_m}{V_{oc} I_{sc}} \quad (1.8)$$

1.4.4 Efficiency (η)

The conversion efficiency is calculated as the ratio between the maximal generated power and the incident power, solar cells are measured under the STC, where the incident light is described by the AM1.5 spectrum and has an irradiance of I_{in} = 1000 W/m^2. [5]

The mathematical expression for solar cell efficiency is:

$$\eta = \frac{V_m I_m}{P_{in}} = \frac{FF\, V_{oc}\, I_{sc}}{P_{in}} \quad (1.9)$$

1.5 Resistive Effects

1.5.1 Series resistance (Rs)

The impact of serial resistance on the current-voltage (I-V) and power-voltage (P-V) characteristics of a solar cell is observed in Figure 1.7. In the domain where the PV cell functions as a voltage regulator, the serial resistance determines the slope of the curve characteristic. The open circuit voltage remains constant, unless the high short circuit current

value is reduced. The increase in the series resistance results in a decrease in the gradient of the curve. Specifically, when the open circuit voltage is increased, an equivalent value is assigned to the short circuit current.[6]

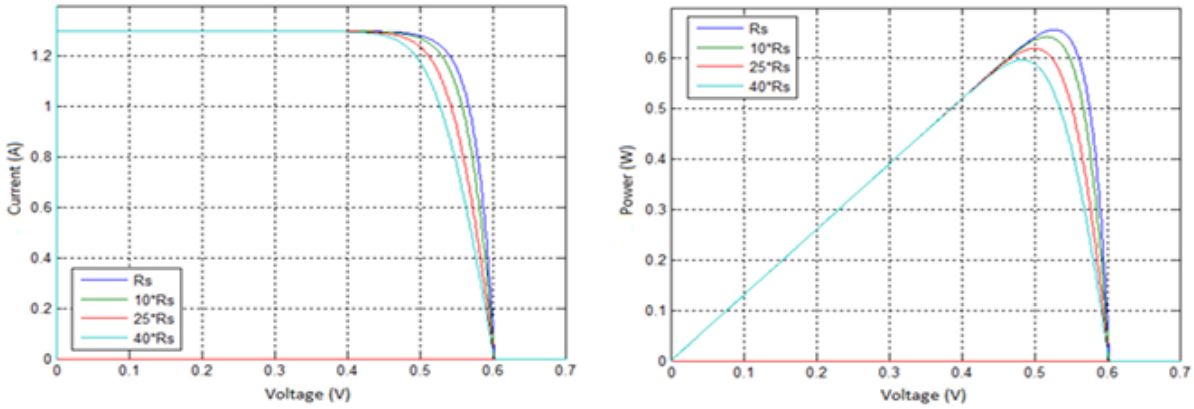

Figure1.7 Influence of series resistance.[6]

1.5.2 Shunt resistance (Rsh)

The shunt resistance accounts for the inevitable current leakage that occurs between the terminals of the solar cells. In general, when the shunt resistance is extremely high, its impact becomes especially noticeable in the generation of power. The presence of shunt resistance causes a slight reduction in the open circuit voltage and enhances the slope of the I-V cell curve in the current operating range (Figure 1.8). [6]

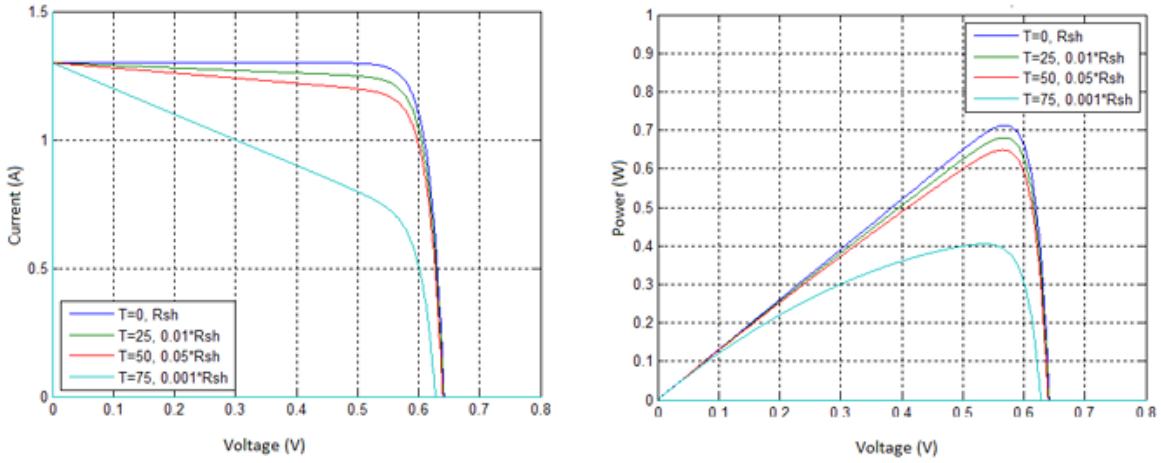

Figure1.8 Influence of shunt resistance [6]

1.5.3 Impact of Both Series and Shunt Resistance

The operational efficacy and overall energy conversion efficiency of photovoltaic cells are markedly influenced by the presence of intrinsic resistances, specifically series resistance () and shunt resistance (). These resistances play pivotal roles in shaping the current-voltage (I-V) characteristics and, consequently, the power output profile of the cells. A detailed comprehension of the impact of and is indispensable for the advancement of cell architecture and the strategic selection of materials to optimize efficiency.

A critical equilibrium must be established wherein is minimized to limit potential voltage drops, and is maximized to inhibit leakage currents. This balance is imperative for the maximization of the cell's power output and its operational efficiency.

1.6 Effect of light intensity

The temperature remains fixed at 25 °C while the irradiance levels are varied (250W/m², 500W/m², 750W/m², 1000W/m²). The I-V and P-V properties under different situations of irradiation are shown in Figure 1.9. The current generated by the solar cell is directly proportional to the level of incident light. Consequently, higher irradiance results in a larger current production. Despite fluctuations in irradiance, voltage remains generally constant. As the level of irradiance increases, there is a clear and immediate impact on the maximum power point: higher levels of irradiance lead to an increase in the maximum power point. [6]

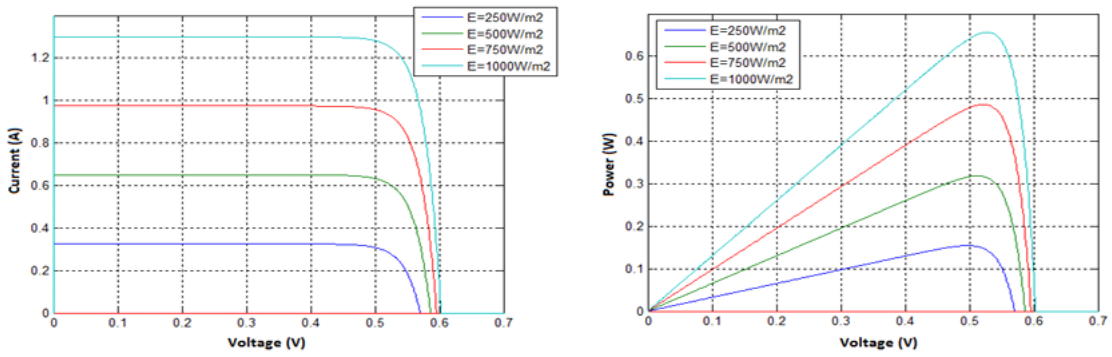

Figure1.9 Influence of the Irradiation [6]

1.7 Effect of Temperature

In contrast, while maintaining a constant irradiance of 1000W/m², the temperature is systematically altered (25 °C, 50 °C, 75 °C, 100 °C) in order to observe its impact on the I-V and P-V characteristic curves of Figure 1.10. The current remains relatively constant as it is mostly determined by irradiance. Nevertheless, a gain in temperature leads to a slight increase in current but causes a decrease in voltage and power output. This suggests that the efficiency of the solar cell diminishes with rising temperatures. The synergistic impact of irradiance and temperature is evident in Figure 1.10, where the influence of elevated temperature is nearly insignificant in comparison to the impacts of irradiance. The power output only exhibits a marginal rise with higher levels of irradiance.[6]

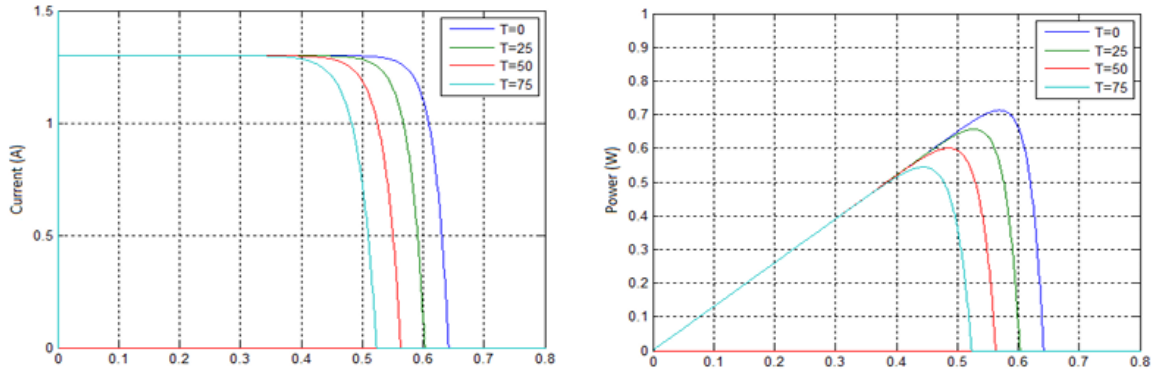

Figure 1.10 Influence of the Temperature [6]

1.8 Conclusion

In conclusion, solar cells work by absorbing light in their active layers, which produces electron-hole pairs that create electrical current via diffusion and drift mechanisms. The basic theoretical foundations of semiconductor physics, which are essential to understand solar cell technology, have been covered in this chapter. The PN junction, which is crucial in determining how solar cells behave, was discussed in detail, with a focus on its characteristics under various circumstances.

In order to clarify various electrical factors, the equivalent electrical circuit of solar cells was also shown. In addition, the effect of temperature was examined, showing how high

temperatures can reduce output voltage and efficiency because of increased rates of carrier recombination and material expansion. Examining how light intensity affects the maximum power point is essential to maximizing solar cell performance across a range of environmental circumstances. Furthermore, the impact of series and shunt resistance was investigated, highlighting their importance in reducing resistive losses and improving overall effectiveness.

CHAPTER 2

Perovskite solar cells

2.1 Introduction

The CH3NH3PbX3 using perovskite solar cells are categorized as "fourth generation" solar technologies [21]. This categorization highlights their pivotal function in transcending the constraints of preceding generations for photovoltaic efficiency and versatility. A hybrid lead trihalide perovskite with exceptional optoelectronic characteristics is CH3NH3PbX3. A halide component, such as iodine (I), chlorine (Cl), or bromine (Br), is represented by the letter 'X' in the formula. Because of these materials' unique properties, they are essential to the development of complex solar systems. [7]

CH3NH3PbX3 exhibits versatility beyond its role in improving solar cell efficiency, as it may also be utilized in other optoelectronic devices such as photodetectors, lasers, and LEDs. CH3NH3PbX3 has significant absorption coefficients that can be precisely adjusted by modifying the halide composition, hence controlling its bandgap. The capacity to adapt allows for considerable enhancements in device performance and fuels ongoing progress in perovskite solar cell technology.

In recent years, there has been a significant improvement in the efficiency of perovskite solar cells. In 2009, the efficiency was only 3.8%, but by 2020, it had climbed to a range of 22.1% to 25%. The remarkable improvements can be attributed to the material's exceptional carrier mobility, excellent absorption coefficient, capacity to withstand defects, and wide range of bandgap tunability [8].

The ensuing sections will cover the basic technologies of perovskite solar cells, the optical characteristics of CH3NH3PbX3, and the significant improvements in solar cell efficiency. We will also examine the thoughtful application of graded bandgap approaches, which have led to a notable increase in the efficiency of these fourth-generation solar cells.

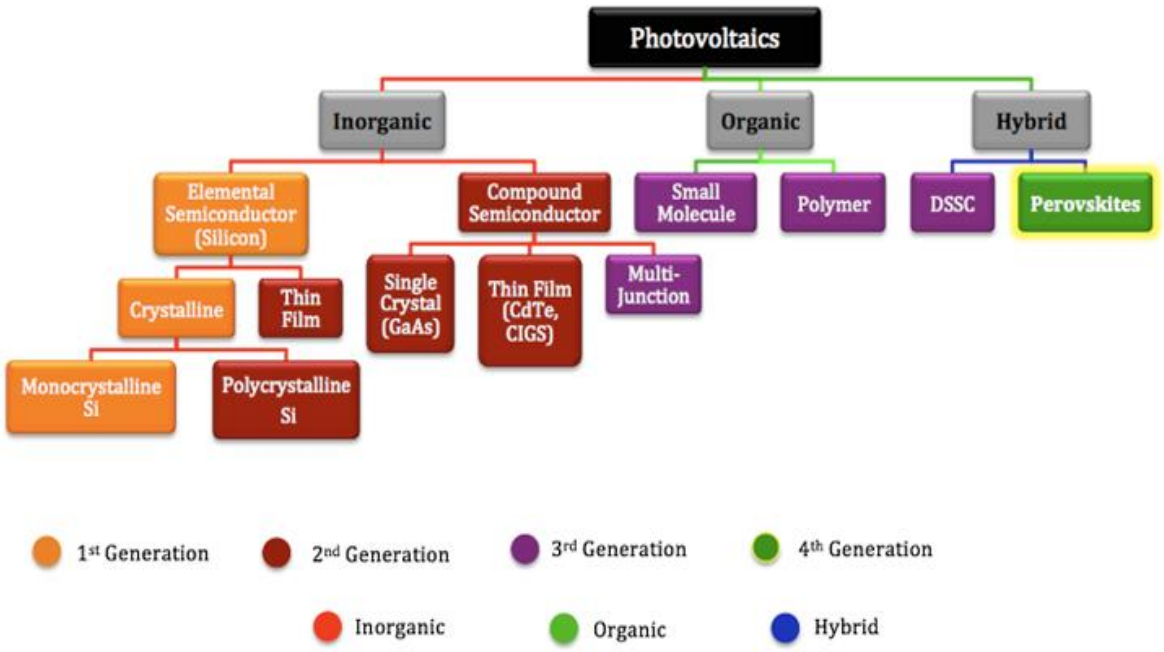

Figure 2.1 Basic classification of photovoltaics.[9]

2.2 CH3NH3PbX3 perovskite light absorber

A hybrid lead trihalide perovskite is CH3NH3PbX3. Iodine (I), chlorine (Cl), or bromine (Br) are examples of halide atoms, and the symbol 'X' in the formula stands for them. The exceptional optoelectronic capabilities of this material have garnered significant recognition [7]. With the use of this chemical materials, advanced photovoltaic technologies can be developed, leading to the creation of solar cells with high efficiency. Its significance also extends to a wide range of optoelectronic uses, including LEDs, lasers, and photodetectors. High absorption coefficients, which may be altered by varying the halide content to alter the bandgap, are a crucial feature of CH3NH3PbX3 that drives continuous improvements in perovskite solar cell technology and also increases the efficiency of photovoltaic systems. These components will be looked at and analysed in the following sections.

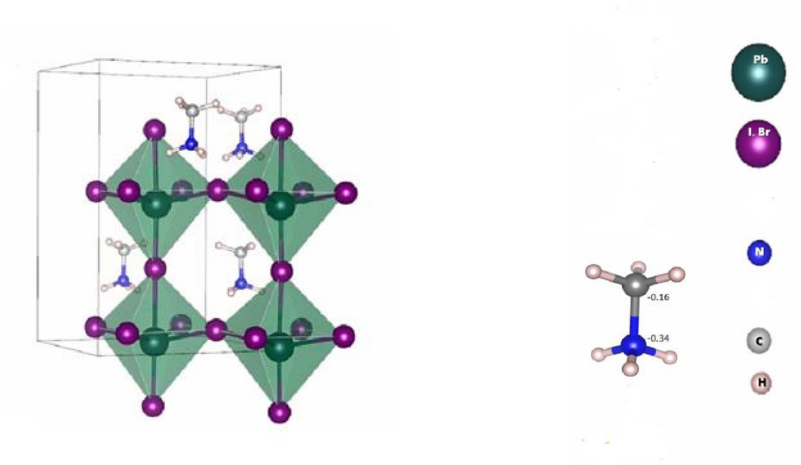

Figure 2.2. Crystal structures of the tetragonal phases of CH3NH3PbX3 where X = I or Br and the partial charges of the used cations [11]

2.2.1 Base technology for perovskite solar cells

The fundamental technology of perovskite solar cells stems from solid-state sensitized solar cells, which were first introduced by O'Regan and Gratzel in 1991 and were based on dye-sensitized Gratzel solar cells. Initially, this technology was designed using a high surface area nanocrystalline TiO2 layer in a photoelectrochemical configuration that was sensitized with molecular dyes. Even though power conversion efficiencies (PCE) of over 12% were attained, there were significant issues with liquid electrolyte leaks. Spiro-MeOTAD, a solid hole conductor, was used in place of the liquid electrolyte to solve this issue. This replacement increased the durability and dependability of dye-sensitized cells while maintaining their basic properties [12].

These basic concepts are combined in a sophisticated way in modern perovskite solar cells (PSCs) with the usage of TiO2 as an electron transport layer (ETL) and Spiro-OMeTAD as a hole transport layer (HTL). Strong charge transport and effective electron-hole pair separation make this structure beneficial and result in higher efficiencies. The efficiency of PSCs has been shown to be significantly increased by annealing treatments of the TiO2 layers. More stability and efficiency gains have been demonstrated when Spiro-OMeTAD is used as a hole transport layer (HTL). Furthermore, the utilization of sophisticated vapor deposition

techniques to produce intricate device designs, such as ITO/TiO2/CH3NH3PbI3-xClx/Spiro-OMeTAD/Ag, has been a recent development made by researchers like Liu et al. With a maximum efficiency of 15.4%, these developments not only improve perovskite solar cells' efficiency but also address critical scalability and manufacturing issues. This makes perovskite solar cells an extremely attractive alternative for energy solutions in the future [13.]

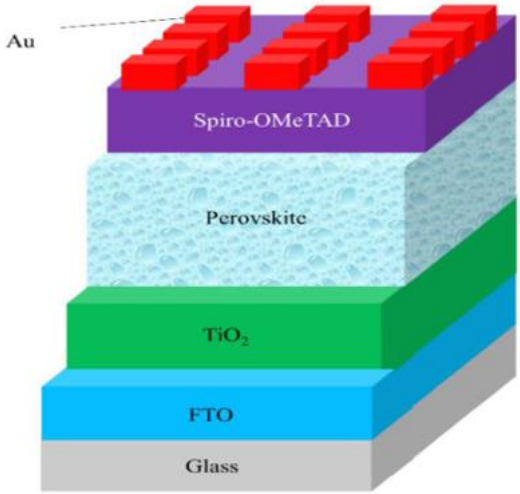

Figure 2.3: The 2-D view of a PSC [17]

2.2.2 Optical properties of CH3NH3PbX3

A broad spectrum of light wavelengths can be absorbed by $CH_3NH_3PbX_3$, especially in the mixed halide form $MAPb(I_{1-x}Br_x)_3$, as demonstrated by its optical properties. This ability is crucial for perovskite solar cells. By varying the halide concentration, these materials' band gaps and light absorption properties can be accurately tuned. Wavelengths of 785 nm, 552 nm, and 580 nm are the absorption onsets of $MAPbI_3$, $MAPbBr_3$, and $MAPb(I_{0.11}Br_{0.89})_3$, respectively. Band gaps at these wavelengths are 1.58 eV, 2.25 eV, and 2.14 eV, respectively. Similar to that of $MAPbBr_3$, the bandgap of $MAPb(I_{0.11}Br_{0.89})$ shows the effect of increased bromine content, which causes a shift of the bandgap towards higher energy levels. Furthermore, increasing the structure's iodine mole ratio enhances its absorption capacity and causes the absorption spectra to shift towards longer wavelengths, which denotes a decrease in the energy gap between the highest occupied and lowest unoccupied molecular orbitals. This

phenomenon is linked to the lattice constant expanding as the iodine content rises, which has an antagonistic effect on the bandgap. The optical characteristics of $CH3NHPbX_3$ perovskites can be altered by varying their composition, which emphasizes its versatility in solar applications. This makes it possible to modify absorption properties in order to maximize solar cell efficiency [15].

2.2.3 Progress in perovskite solar cells

The efficiency, stability, and manufacturing processes of perovskite solar cells (PSCs) have improved significantly, making them a major focus of interest for the photovoltaic research community. In recent years, the efficiency of devices based on perovskites has increased significantly, approaching 25%. This accomplishment is attributable to developments in the fabrication processes, device architecture, and perovskite crystal structure. Through the modification of band gap characteristics, the transmittance, carrier mobility, and commercialization potential have been enhanced by using multiple layers, such as buffer layers and electron transport layers [14].

Notable material Spiro-OMeTAD has demonstrated remarkable efficacy when used as a hole transport layer (HTL) to improve the functionality and efficiency of solar cells. These features have been further enhanced by the introduction of dopants, which has resulted in the device's overall optimization. Furthermore, compared to regular $MAPbI_3$, mixed halide perovskites like $MAPb(I_{1-x}\ Cl_x)_3$ have shown better electron-hole diffusion lengths. As a result, carrier dynamics are enhanced. Both $MAPb(I_{1-x}Br_x)_3$ and $MAPb(I_{1-x}\ Cl_x)_3$ are more beneficial for practical application since they can be synthesized at room temperature and have demonstrated increased carrier mobility and decreased carrier recombination rates [14].

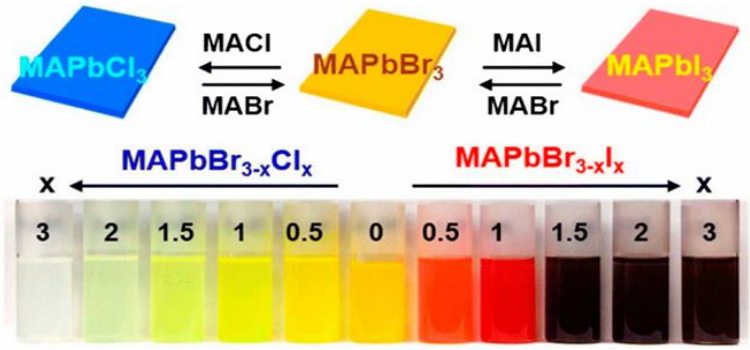

Figure 2.4 Snapshots of halide replacement/mixing in the perovskite assembly (reproduced with permission from ref. 66, copyright 2014 ACS).[14]

Furthermore, the utilization of triple or quadruple cation mixtures is meant to further improve efficiency and stability. Furthermore, because of their enhanced stability and low processing temperature, materials like titanium oxide have been used extensively as electron transport layers (ETLs). This highlights the ongoing quest for perovskite solar cells' (PSCs) more stable and effective constituents. Generally speaking, perovskite solar cell technology is always evolving, with a focus on resolving material stability concerns and enhancing efficiency. The potential of perovskite solar cells in the field of renewable energy is being pushed by this advancement [14].

2.3 Graded energy band for efficient solar cells

In order to create graded energy bands in solar cells, the bandgaps of many layers including the active perovskite layer, the electron transport layer (ETL), and the hole transport layer (HTL) are adjusted so that the device's performance is maximized and charge collecting efficiency is increased. By employing sophisticated band grading methods in these layers, the flow of holes is improved, recombination is reduced improving the stability and performance of solar cells.

2.3.1 Graded band for ETL

In order to enhance the efficiency of perovskite solar cells (PSCs), it is essential to carefully engineer the band structure of the electron transport layer (ETL). In order to achieve

successful electron extraction and prevent electron backflow, the conduction band (CB) of the perovskite must be positioned at a higher energy level than that of the electron transport layer (ETL). Similarly, for effective carrier transfer, the valence band (VB) of the perovskite should be positioned at a lower energy level than that of the hole transport layer (HTL).

The ETL's graded band structure is considered as one of the factors in raising PSC efficiency. Typically, heterojunction bilayers are used to achieve this structure because they reduce energy dissipation and enable the selective transport of carriers. These bilayers are usually composed of inorganic material mixes such as TiO_2/ZnO or TiO_2/SnO_2. These materials were chosen because of their outstanding stability, excellent electron mobility, and capacity to form effective ohmic contact with adjacent layers.

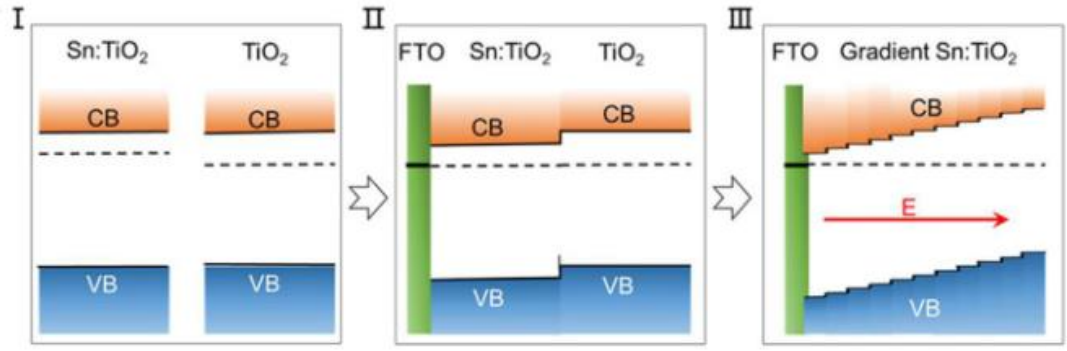

Figure 2.5 Schematic of band structure of gradient Sn doped TiO2

Graded band ETLs are designed so that the energy bands vary progressively as the thickness of the ETL increases. This may entail adjusting the doping levels, altering the proportions of different materials, or employing a bilayer structure where each layer is specifically tailored to achieve a desired band alignment. The progressive alteration in the conduction band levels across the electron transport layer (ETL) aids in diminishing the potential barriers that electrons must surmount. This can augment the overall efficiency of the solar cell and mitigate energy loss caused by recombination.

A band offset of approximately 0.2 eV is ensured between the perovskite layer and the electron transport layer (ETL) by the graded band structure. The small divergence is crucial because it reduces energy loss during electron transit, increasing the solar cell's total efficiency. Furthermore, several fabrication methods can be applied to heterojunction bilayers to get the

desired band alignment. For instance, precisely tailored graded band structures can be produced by combining atomic layer deposition (ALD) with spin-coating or by using sol-gel methods with nanoparticle precursors, as shown in figure 2.1.

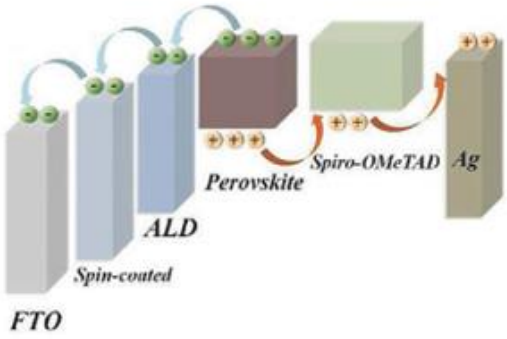

Figure 2.6 Energy-level diagram based onspin-coated/ALDTiO2 homojunction ETL

To summarize, the manipulation of graded band structures in the electron transport layer (ETL) of perovskite solar cells (PSCs) is a basic method to improve their efficiency in converting sunlight into electricity. By meticulously choosing materials and employing advanced fabrication techniques, it is feasible to optimize the electron transport layer (ETL) in order to facilitate efficient electron flow, improve carrier separation, and eventually raise the energy conversion efficiency of perovskite solar cells [16].

2.3.2 Graded band for HTL

In perovskite solar cells, the role of the p-type hole-transporting layer (HTL) is to remove holes from the perovskite layer while blocking the flow of electrons in order to enhance photovoltaic efficiency (PCE) and lower energy loss.

Advancements in HTL materials can maximize the efficiency of solar cells. Gradient energy level implementation in the HTL has proven effective in fulfilling the varied demands of different operating conditions. For instance, Han's application of a graded band structure rGO/PTAA bilayer as the hole transport layer (HTL) resulted in a notable increase in power conversion efficiency (PCE) to 17.2%. Other bilayer hole transport layers (HTLs) with significant potential in photoelectric devices include PEDOT/black phosphorus quantum dots,

black phosphorus/CuSCN, c-NiOx/m-CuGaO2, and CuO2/CuO. This is explained by their ability to create a constant energy level gradient which enhances charge carrier mobility [16].

In addition, co-annealing procedures have been devised to seamlessly incorporate HTL elements into the perovskite layer. Li et al achieved the formation of a continuous gradient of Spiro-OMeTAD doping at the perovskite/HTL interface by dissolving Spiro-OMeTAD in chlorobenzene. This method optimizes the characteristics of the interface and improves the efficiency of solar cells [16].

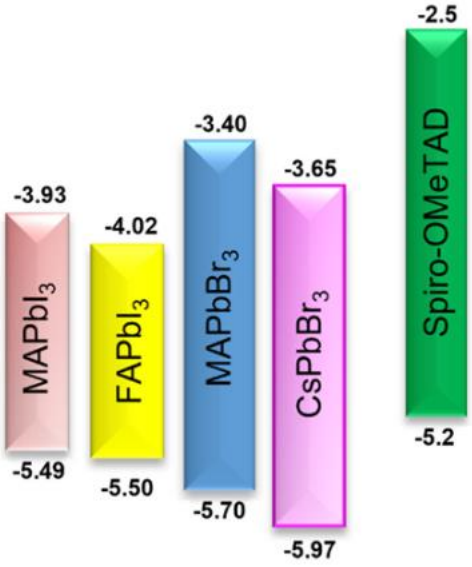

Figure 2.7 Energy levels of various lead halide perovskites and spiro-OMeTAD [10]

When choosing materials for the HTL, it is crucial to guarantee the long-term durability and effectiveness of the solar cell. The essential attributes encompass an appropriate redox potential for the rejuvenation of quantum dots and the sustenance of a high voltage output (Voc), little corrosiveness to ensure durability, elevated ionic conductivity for effective hole transfer, complete regenerativity, and superior transparency and stability under visible light. These parameters are crucial for the development of HTL materials that can satisfy the requirements of high-performance photovoltaic devices [18].

2.3.3 Graded band for perovskite

In recent developments in perovskite solar cell technology, a crucial approach to improve the performance of the devices is the compositional grading of the perovskite material. The process consists of using a basic chemical treatment, where an organic bromide solution such as MABr or FABr is applied in a thin layer onto primary absorbers like MAPbI3 or FAPbI3 via a spinning process. This technique initiates a partial substitution of halide ions, leading to the formation of a concentration gradient of bromide ions (Br) throughout the thickness of the absorber. The resulting graded bandgap has a significant impact on the features of the solar cell by improving charge collection and minimizing interface recombination [19].

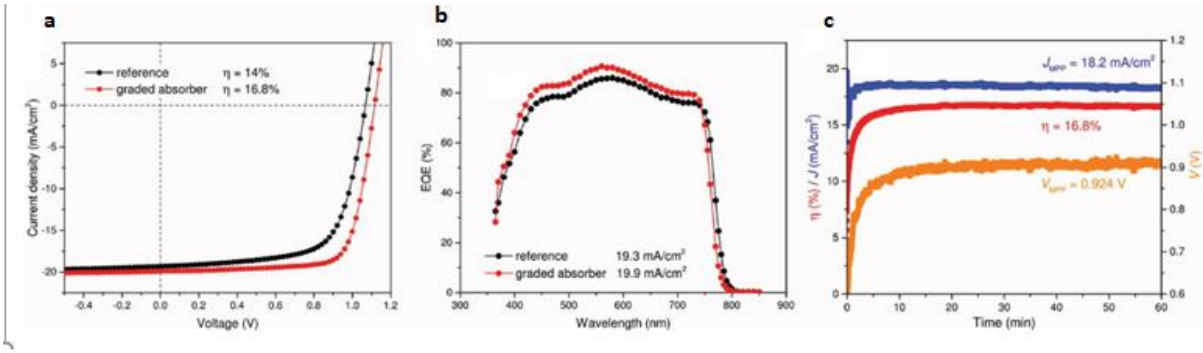

Figure 2.8 Photovoltaic performances of graded $MAPb(I_{1-x}Br_x)_3$ perovskite solar cells [19]

A similar concept has long been employed in silicon solar technology. Tunnelling insulators or back surface fields created by high doping enable the employment of chemical and/or field effect passivation in this process. With the use of hydrogen bromide (HBr) fume replacement doping, a constant concentration gradient of Br across the perovskite absorber has been successfully established in perovskite solar cells. This method allows Br to be incorporated into the perovskite structure in a controlled manner. It is important to note that ion migration and intermixing mechanisms cause the Br gradient created by this method to eventually change into a homogeneous mixed halide layer. The stability and efficiency of the solar cells in the long run may be impacted by this change.

2.3.4 Bandgap tuning method

A sequential deposition process effectively demonstrates bandgap tuning in mixed anion lead halide perovskites $MAPb(I_{1-x}\ Br_x)_3$, where $0 \leq x \leq 1$. By soaking PbI_2 films in a pure MABr solution for varying times (0.5, 5, 10, and 20 minutes), the absorption edge of perovskite films was systematically moved to higher energies. The absorption edge in Figure 1 had matching

wavelengths of 660 nm, 645 nm, 625 nm, and 556 nm, which matched bandgaps of 1.89 eV, 1.92 eV, 1.98 eV, and 2.23 eV, in that order. This shift shows that the bandgap can be changed by adjusting the halide precursor's composition and the amount of time it is immersed in the precursor solution. Moreover, further evidence for these alterations is provided by the UV-Vis absorption spectra of $MAPb(I_{1-x}\ Br_x)_3$ shown on figure 2.9.

Consequently, the hue of the MAPbI3 perovskite films underwent a transition from dark brown/black to red to orange, as shown in Figure 2.9.

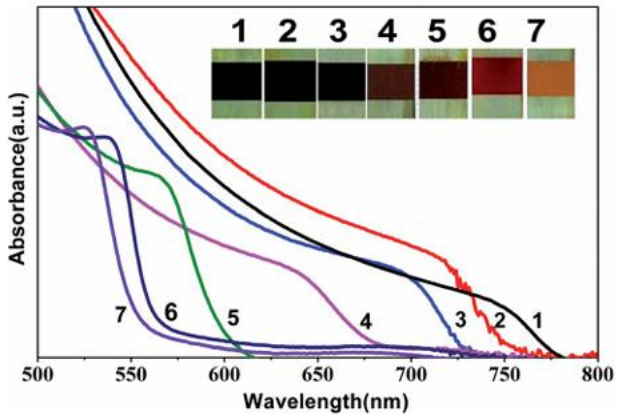

Figure 2.9 UV-Vis absorption spectra of the mixed halide lead perovskite $MAPb(I_{1-x}\ Br_x)_3$ ($0x\leq1$))films formed via a sequential deposition process [20]

To maximize the performance and utility of perovskite materials in solar cells, bandgap adjustment is essential [20].

Table 2.1 summarizes the measured bandgap values for different compositions of halides (iodide/bromide) in the perovskite film according to relation (2.1) where x represents the amount of bromide in the halide mixture.

$$Eg(x) = 1.57 + 0.39x + 0.33 \qquad (2.1)$$

Table 2.1 Variation in volume and molar ratio of MAI and MABr, measured bandgap and estimated composition of halides (iodide/bromide) in the perovskite film.

Film N°	MAI:MABr (v/v)	MAI:MABr (moles)	Measured bandgap (eV)	Estimated composition of films
1	1:0	--	1.56	MAPbI3
2	4:0	2.85	1.62	MAPb()$_3$
3	2:1	1.42	1.69	MAPb()$_3$
4	1:1	0.70	1.79	MAPb()$_3$
5	1:2	0.35	1.96	MAPb()$_3$
6	1:4	0.17	2.01	MAPb()$_3$
7	0:1	--	2.23	MAPb()$_3$

2.4 Conclusion

Throughout this chapter, CH3NH3PbX$_3$ has been highlighted as a ground-breaking component in the field of photovoltaic technology, underscoring its vital role as a highly effective light absorber. The next generation of perovskite solar cells is based on hybrid lead trihalide perovskite, which is recognized for its versatile halide components and outstanding optoelectronic properties. By precisely adjusting the bandgap of CH3NH3PbX3 by halide alteration, perovskite solar cells' optical properties have been improved, resulting in significant increases in their efficiency and scalability.

The creation of graded energy bands in the perovskite layer, the electron transport layer (ETL), and the hole transport layer (HTL) has greatly increased the functionality and efficiency of solar cells. Specialized applications have been used to accomplish these advantages. The alignment of the energy levels across the solar cell has been made possible by techniques like bandgap tuning and deliberate band grading, which have improved charge transfer and reduced recombination losses to increase overall efficiency.

Because of their high efficiency and low production costs, perovskite solar cells have the potential to revolutionize the solar power industry. Continuous research and development in this area could lead to more sustainable and commercially viable solar energy solutions globally, as well as improvements in the technical properties of these solar cells. Leading the way in solar technology advancement for a more sustainable and efficient future is CH3NH3PbX3

CHAPTER 3

Numerical simulation, Results and discussion

3.1 Introduction

One very useful tool for simulating semiconductor devices such as MAPbI3 and perovskite solar cells is Silvaco TCAD Simulator. We can model and simulate basic properties such as current density-voltage (J(V)) and power-voltage (P(V)) relationships by defining the device structure with specific layers, connection creation and related physical model applications. We can also calculate photoelectric metrics such as efficiency (η), filling factor (FF), open-circuit voltage (Voc), and short-circuit current density (Jsc).

3.2 Silvaco Tcad simulator

3.2.1 Overview

Silvaco TCAD Simulator is a powerful feature-rich software developed by Silvaco Inc. It has been designed for the simulation and testing semiconductor devices, sophisticated materials such as perovskites, as well as various semiconductor structures and materials such as transistors, diodes and solar cells. This Simulator is a widely used tool for device design, fabrication networks and complex physical materials models to simulate electrical, optical and thermal behaviour, applications in transient analysis and new semiconductor manufacturing. Its ability to provide deeper insights into device performance, improve design features and understanding of complex physical processes are some of its key features, making it an essential tool for advancing next-generation semiconductor technologies. The figure above shows the types of information that flow in and out of Atlas.

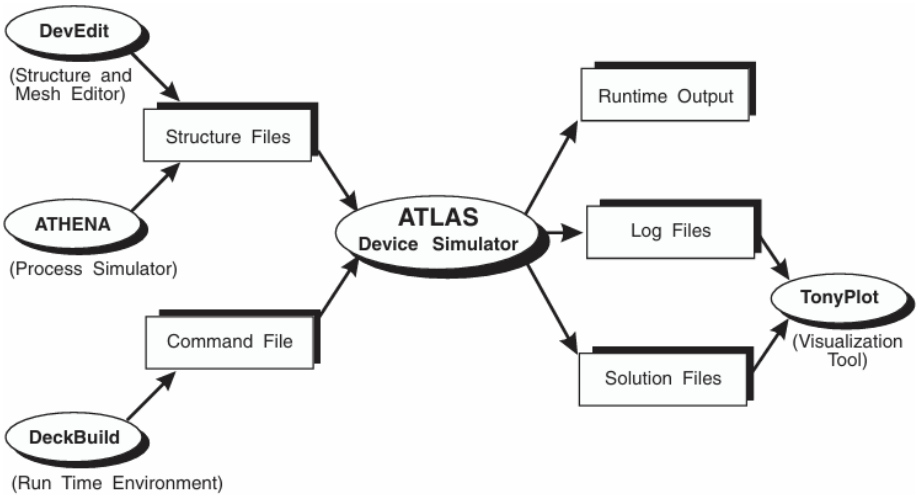

Figure 3.1: ATLAS Inputs and Outputs [25]

3.2.2 Running Atlas in the Deckbuild

The first line the program typically reads is a statement that sets up the simulation state or starts the simulation. This line is usually accompanied by the GO ATLAS command, a command that tells ATLAS to begin processing subsequent commands in the script, starting the simulation process.

3.2.3 Input File Structure

The order in which the information appears in the ATLAS input file is very important. There are five types of words that must have the correct structure (figure 3.2), otherwise, an error message is displayed, which may cause the program to malfunction or terminate. For example, if material parameters or models are set in the wrong order, they may not be used in calculations.

Network definitions, configuration definitions, and specifications in different solutions are also important. Otherwise, poor implementation or interruption of the program may also occur [25].

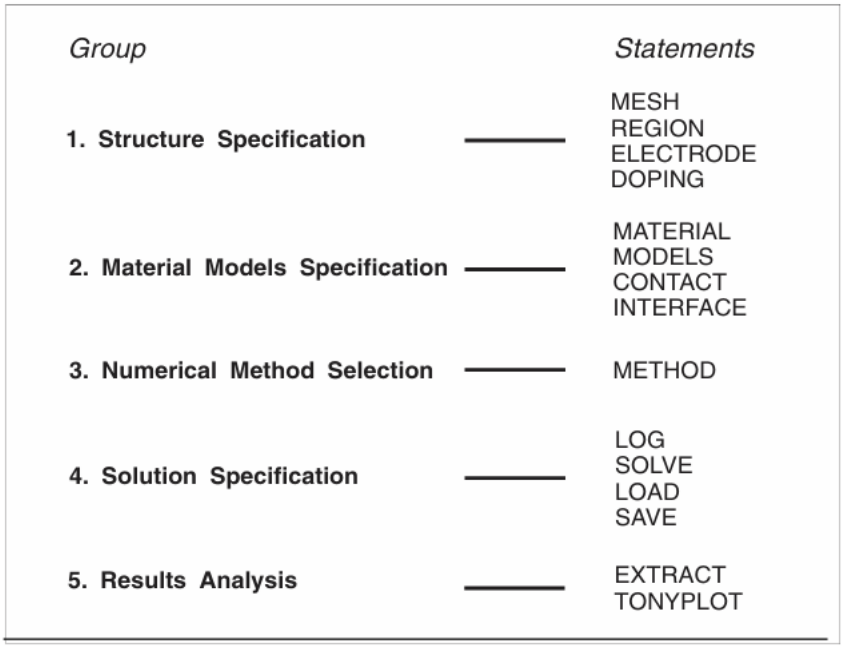

Figure 3.2: ATLAS Command Groups with the Primary Statements in each Group

Every statement in atlas software has the following format:

<keyword> <parameter>=<value>

• <keyword>: A specific command recognized by the system, dictating the action to perform.

• <parameter>: An attribute of the action, specifying what aspect is affected.

• <value>: The specific setting applied to the parameter.

3.2.3.1 Structure specification

Silvaco's ATLAS application arranges command groups to make simulation setup and operation simpler. Groups provide for complex control and configuration by containing a set of commands related to specific aspects of the simulation.

► MESH:

Begin by defining the mesh that covers the physical simulation domain. This mesh is outlined by a series of horizontal and vertical lines where their spacing is detailed according to the following commands:

X.MESH LOCATION = <VALUE> SPACING = <VALUE>

Y. MESH LOCATION = <VALUE> SPACING = <VALUE>

Example:

X.MESH LOCATION = 0 SPACING = 0.1

Y. MESH LOCATION = 0 SPACING = 0.1

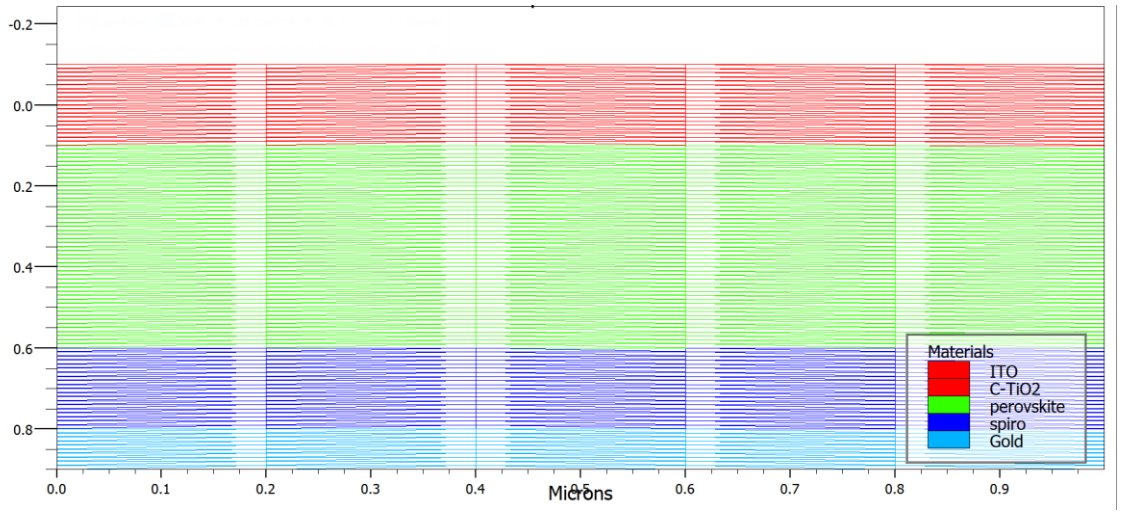

Figure3.3 Typical perovskite solar cell structure mesh

►REGION

The process of defining regions in ATLAS is essential since it entails defining several semiconductor device components, including distinct layers, doping profiles, or material kinds. The material and electrical parameters of each region are described, and these are essential for accurately replicating device behaviour. The definition of a region in ATLAS follows these steps:

Region number = <integer> <material type> <position parameter>

Example:

REGION num=3 user. Material = MAPbI3 user. Group = semiconductor x.min = 0 x.max = 1 y.min = 0.6 y.max = 1.2

►ELECTRODE

Using the ELECTRODE statement, we can define at least one electrode that makes contact with a semiconductor material in the Silvaco ATLAS simulation program. Here are some essential details regarding electrode specification:

- A maximum of 50 distinct electrodes can be specified. Microns are used to provide position parameters like X.MIN, X.MAX, Y.MIN and Y.MAX.
- The terms LEFT, RIGHT, TOP, and BOTTOM allow a fast definition of the electrode location.

The format to define electrodes is: electrode name = <electrode name> <position parameters>

Example:

ELECTRODE NUM = 1 NAME = cathode TOP MATERIAL = ITO x.min = 0 x.max = 1 y.min = 0 y.max = 0.5

ELEC NUM = 2 NAME = anode BOTTOM MATERIAL= gold x.min = 0 x.max = 1 y.min = 1.3 y.max = 1.35

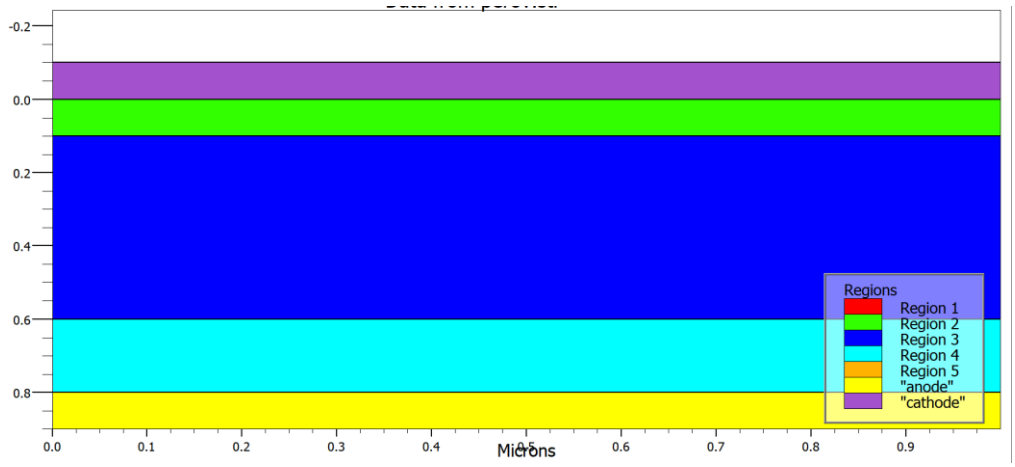

Figure 3.4 Regions and electrodes specification of a typical perovskite solar cell

► DOPING

Within Silvaco ATLAS, users can define doping profiles through analytical methods or by importing them from process simulation or experimental data files using the following format.

Doping <distribution_type> <dopant_type> <position parameters>

Example

Doping uniform concentration = 1e16 N.type region = 1

Doping gaussian concentration=1e18 P.type x.left = 0.0 x.right = 1.0 peak = 0.1

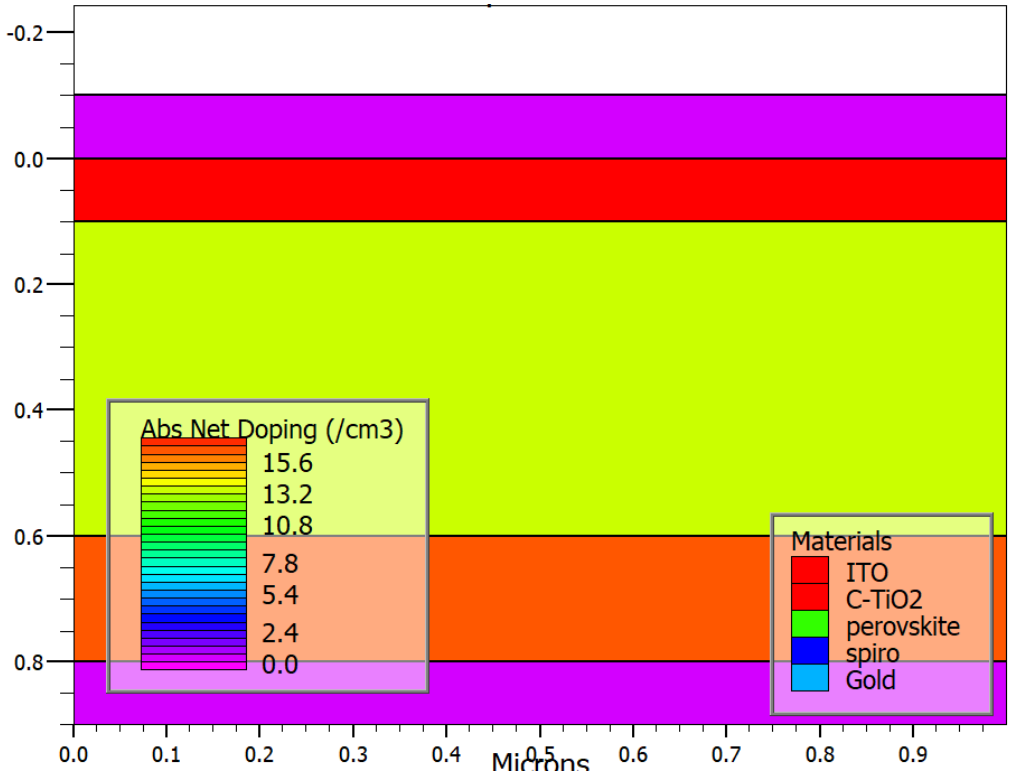

Figure 3.5 Doping specification of typical perovskite solar cell

3.2.3.2 Materials Model specification

►MATERIAL

The MATERIAL statement can be used by the Silvaco ATLAS program to define material qualities. With the use of this capability, users can designate particular parameters for various material classes, such as conductors, insulators and semiconductors. The format to define material is as follows

material <localization> <material_definition>

Example:

Material mat=MAPbI3 user.group=semiconductor user.default = Silicon Taun0 = 1e-6 \

Taup0 = 1e-6 mun = 1 mup = 1 nc300 = 1e19 nv300 = 1e17 eg300 = 1.55 affinity = 3.8 permi = 100

► MODEL

The physical models fall into five categories: mobility, recombination, carrier statistics impactionization and tunnelling. The syntax of model statement is as follow: models <model flag> <general parameter > <model dependent parameters>

Example

Model SRH Auger fermi fldmob conmob

3.2.3.3 Numerical method selection

There are several numerical techniques for determining answers. Three primary numerical techniques are frequently employed in Silvaco Atlas to solve the systems of equations following the materials model specification: the Block approach, the Newton method, and the Gummel method.

3.2.3.4 Solution specification

► LOG

The ATLAS User's Manual describes how to retain all terminal attributes and save simulation run V-I (voltage-current) curve data into a file using the LOG command according to the following syntax:
LOG outfile = <filename>

Example:

LOG outfile = Mcil.log

►SOLVE

Specific bias spots are found using the SOLVE statement. To accomplish convergence for the equations required to calculate bias points with a step size of 0.01 and a range of 0 V to 1.2 V, the code snippet that follows is utilized.

Solve vanode = 0.0 name = anode vstep = 0.01 vfinal = 1.2 b1=1

► LOAD

Importing previously saved solution files is done with the LOAD command. This capability might be useful for starting a simulation from a specified point in time or for continuing simulations from a previous execution. The essential syntax is as follows:

LOAD INFILE=name of file

Open INFILE as data1.str.

► SAVE

The Save statement is used to save the results of simulations into files that can be used for data analysis and visualization, or for use in additional simulations. The basic framework is shown below:

Syntax: Save_outfile = filename

Example:

Save data1.str as outfile

3.2.4 Results analysis

►EXTRACT, TONYPLOT

To obtain the necessary curves and features, the EXTRACT and TONYPLOT statements are employed. The example below shows the extract statement to obtain the current-voltage characteristic curve of a solar cell and the resulting data are saved into the IV.dat file. Next, these data are represented in a graph using the Tonyplot statement.

extract name = "IV" curve(v."anode",i."anode"*1e08*1e03) outfile = "IV.dat"

Tonyplot IV.dat

3.3 Solar cell structure

The schematic layout of a standard perovskite solar cell, featuring layers that are respectively: the TCO (Transparent Conducting Oxide) layer, which is usually composed of materials such as Indium Tin Oxide (ITO) and permits light to flow through the cell, the HTM (Hole Transport Material) layer comes next, which makes it easier for holes “positive charge

carriers" to move within the perovskite layer. Both charge production and light absorption take place in the core perovskite layer. The ETM (Electron Transport Material) layer sits above the perovskite layer and facilitates the transfer of electrons "negative charge carriers" out of the layer. The metal layer, which is the topmost layer and is typically composed of metals like silver or gold, is what gathers the electrons to complete the electrical circuit. The cell's overall performance is maximized by the vertical arrangement of these layers, which guarantees excellent light absorption and charge transmission.

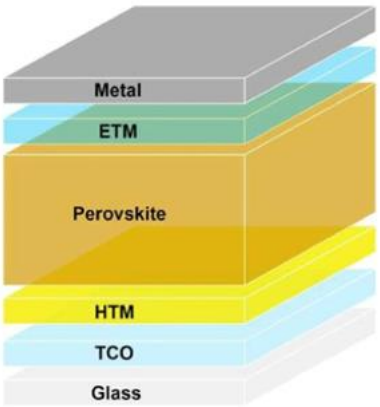

Figure 3.6 Schematic layout of a standard perovskite solar cell

3.4 Numerical simulation of the studied perovskite solar cell

Several essential layers make up the structure of a typical perovskite solar cell, which is perfect for simulation in SILVACO ATLAS. Each of these layers serves a particular purpose. Beginning with the top, or light incident side, the anode is often composed of transparent conducting oxide, such as indium tin oxide (ITO), which collects and transfers holes to the external circuit while facilitating light ingress. It typically has a thickness of between 100 and 200 nm. Next, comes the 100–200 nm thick Hole Transport Layer (HTL), which is mainly made of Spiro-OMeTAD. Its purpose is to help move holes from the perovskite layer to the anode by obstructing electrons and reducing recombination at the anode contact.

The Active Layer, located in the middle of the cell, is made up of a 300 – 500 nm-thick perovskite materials similar to methylammonium lead iodide ($CH_3NH_3PbI_3$). This layer

effectively creates electron-hole pairs by absorbing sunlight. The Electron Transport Layer (ETL) sits below the active layer. It is composed of compact titanium oxide (C-TiO_2) and is between 50 and 100 nm thick. Its purpose is to transport electrons to the cathode while blocking hole passage. The cathode, which serves to gather electrons and complete the external circuit, is the final component of the structure. It is often a thin layer of gold or another appropriate metal. To achieve high efficiency solar power conversion, light absorption, charge carrier separation, and transport processes are optimised by this meticulously constructed architecture.

For simulation in SILVACO ATLAS, the operational conditions must be specified. In the common testing conditions, the complete device is usually simulated at a temperature of 300 K and exposed to a solar spectrum comparable to AM1.5 (Air Mass 1.5), which is a standard for testing in natural sunlight circumstances and replicates the solar irradiance of sunlight through the Earth's atmosphere. These prerequisites guarantee that the simulation accurately captures the impact of the environment on the operation of the solar cell, enabling precise analysis and stability and efficiency optimisation. Each layer's properties are presented in Table 3.1.

3.5 Parameters used in the simulation

3.5.1 Physical and geometric parameters

The table below presents the geometric and physical properties of different materials (Spiro-OMeTAD, MAPbI3, and C-TiO2) used in the studied solar cell.

Table (3.1): Solar cell layer parameters based on MAPbI3 [23].

Layer	Spiro-OMeTAD	MAPbI3	C-TiO2
Thickness (µm)	100	600	100
Bandgap Energy (eV)	3.00	1.55	3.2
Electron Affinity (eV)	2.45	3.8	4
Permittivity (F/m)	3	100	19
Hole Mobility (cm^2/Vs)	2.0×10^{-3}	1	0.1

Electron Mobility (cm^2/Vs)	2.0×10^{-3}	1	0.2
Hole Life time (s)	10^{-7}	10^{-6}	10^{-7}
Electron Life time (s)	10^{-7}	10^{-6}	10^{-7}
N_C	2×10^{18}	10^{19}	2×10^{18}
N_V	2×10^{19}	10^{17}	2×10^{19}

3.5.2 Optical parameters

The first and essential step in the photoelectric conversion process is photon absorption. Thus, an important physical property measured in a photoelectric semiconductor material is its absorption coefficient (α), expressed in units cm^{-1}. Figure (III.1) shows the variation of these parameters over a range of wavelengths in the visible spectrum using Atlas Silvaco.

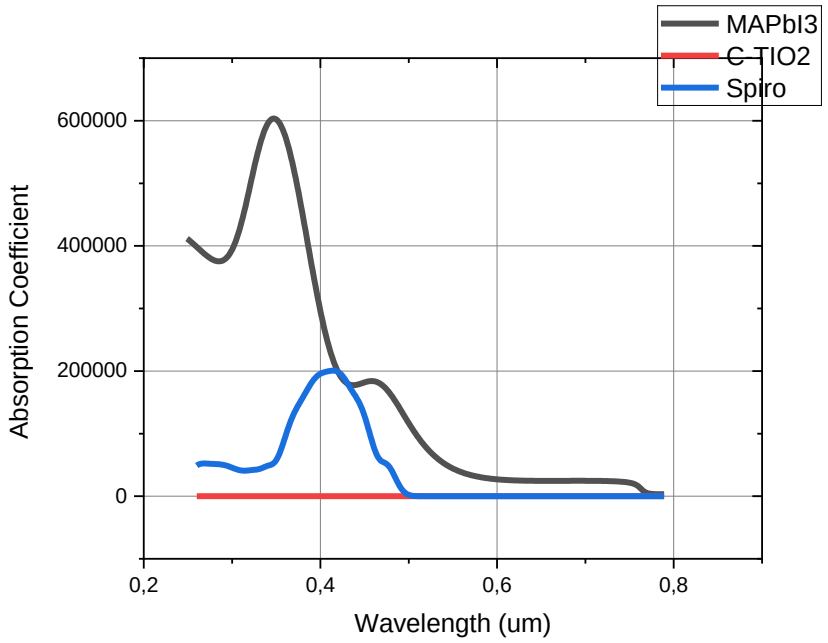

Figure 3.7 Absorption coefficients of the three layers

MAPbI3 demonstrates substantial absorption in the visible light spectrum, with a notable absorption peak appearing at a distance of roughly 0.4 to 0.6 micrometers. For solar cells to effectively absorb sunlight, this characteristic is necessary. Throughout the spectrum, C-TiO2 has a significantly lower absorption coefficient, consistent with its role as an electron

transport layer. To optimize light penetration to the active layer, it should ideally be transparent to incoming light. Spiro-OMeTAD exhibits low absorption in the visible range, making it an appropriate material for a hole transporter so that holes move more easily without absorbing a large amount of incident light.

3.6 Photovoltaic performances

The efficiency of photovoltaic (PV) systems is an important determinant of the performance and efficiency of solar cells. To understand these achievements, it is important to examine the electrical properties and thermal properties of the cells.

3.6.1 J(V) and P(V) characteristics

The characteristics of the current density J(V) and the power density P(V) of the cell are respectively shown in figures (3.8) and (3.9). The results are consistent with previous findings [20].

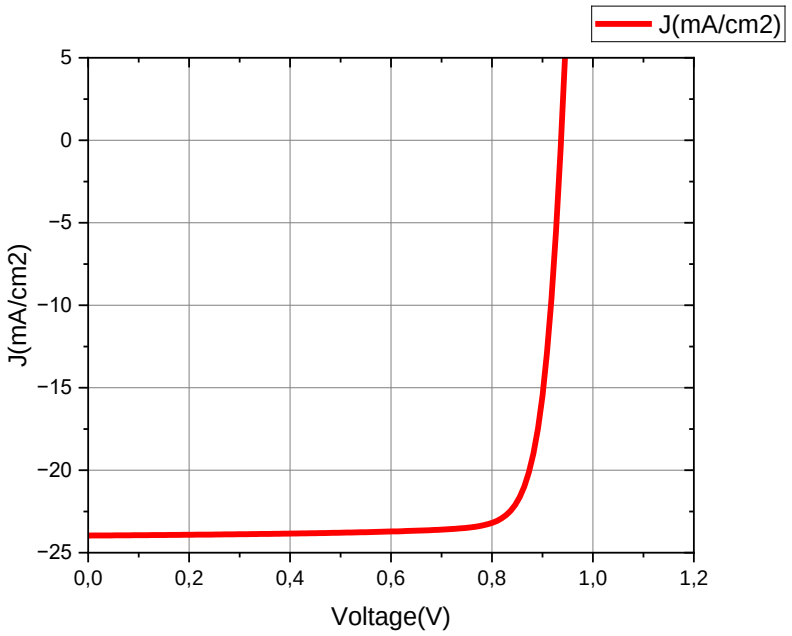

Figure 3.8 Current density-voltage (J-V) curve of the solar cell

The curve demonstrates that power generation occurs as the voltage rises from 0 since the current density is largely constant and negative. The current density abruptly increases and

shifts to positive values indicating the approach of the open-circuit voltage (Voc) which approaches 0.936872 volts.

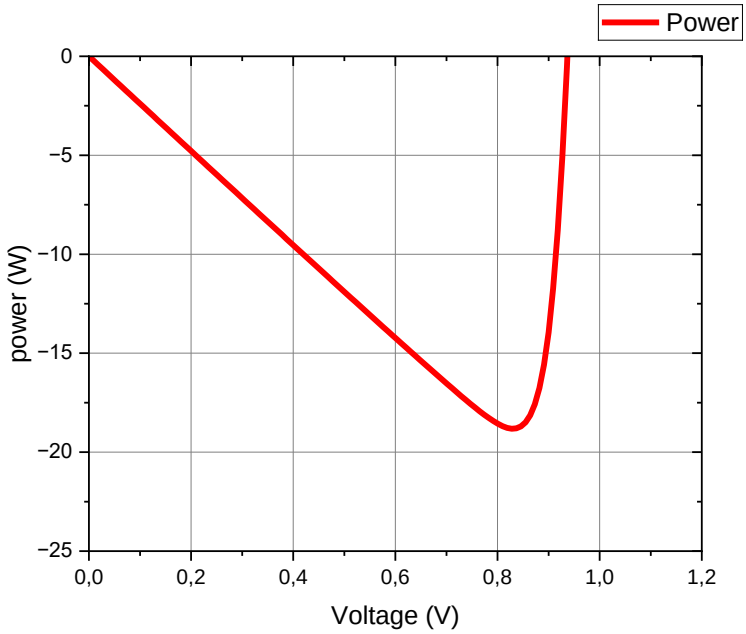

Figure 3.9 Power curve of the solar cell

In figure 3.9, the curve shows that power grows first when voltage rises from zero, achieving the solar cell's maximum power output reaching the maximum power point (MPP), where the product of current and voltage (the power output) is at its maximum. This point, which denotes the ideal operating condition for the cell to supply the highest amount of electricity to a load, is crucial for solar cell efficiency. As the voltage approaches the open-circuit voltage (Voc), which is the point at which no current flows in an open circuit, the power rapidly decreases beyond the MPP.

3.6.2 Photovoltaic parameters (Jsc, Voc, FF and PCE)

The short-circuit current density (Jsc), the open-circuit voltage (Voc), the fill factor (FF) and the conversion efficiency (PCE) are among the crucial performances for evaluating the effectiveness and performance of solar cells. Using the J-V curve, these parameters are summarized in table 3.2.

Table 3.2: Performances of the solar cell

Jsc(mA/cm2)	Voc (V)	FF(%)	PCE(%)
23.96	0.94	83.80	18.81

3.7 Solar cell with a graded energy bandgap

3.7.1 Substitution of Br to I for a graded absorber

The bandgap of the perovskite material is significantly impacted by the addition of bromine (Br) to $MAPbI_3$ to create $MAPb(I_{1-x}Br_x)_3$. It has been found that the valence band can be tuned by changing the Br content, giving fine control over the perovskite absorber's bandgap. Consequently, adding Br to $MAPbI_3$ broadens the bandgap, which is advantageous for maximizing the electrical and light absorbing capabilities of perovskite-based solar cells.

3.7.2 Spectral response of the cell with the uniform gap

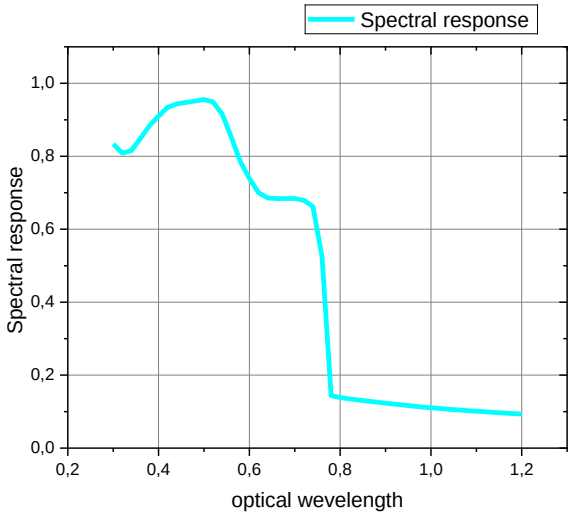

Figure 3.10 Spectral response of the cell

The graph displays the graded perovskite solar cell's External Quantum Efficiency (EQE) at different optical wavelengths. The efficiency with which photons of various wavelengths are transformed into electrical charges is measured by the EQE. The graph shows that the EQE peaks at approximately 550 nm, which is inside the visible light spectrum. This means that this solar cell can convert light most efficiently at a wavelength of over 550 nm, with an efficiency of over 80%. The efficiency sharply decreases beyond 750 nm and

approaches zero beyond 1000 nm, indicating the cell's low sensitivity to near-infrared light. This data, which shows how well the cell can yield solar energy across various light spectrums, is essential for assessing the cell's performance and adjusting it for certain lighting situations.

3.7.3 Simulation of the gap graded solar cell

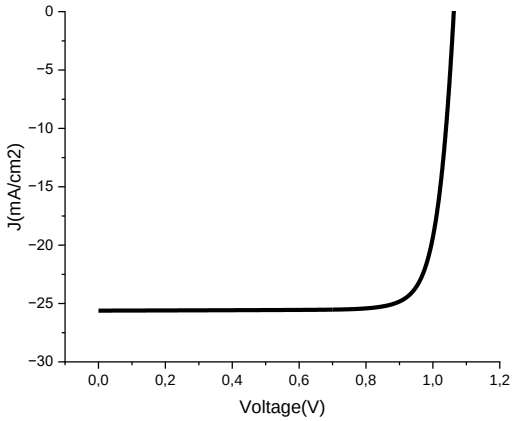

Figure 3.11 J-V characteristic of the graded perovskite solar cell

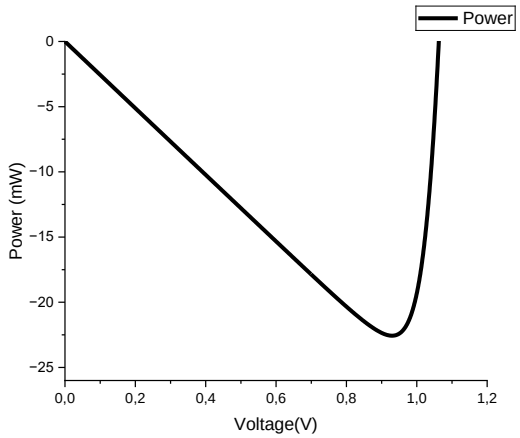

Figure 3.12: P-V characteristic of the graded perovskite solar cell

The extracted external parameters of the solar cell from J-V and P-V characteristics are presented in table 3.3.

Table 3.3: Photovoltaic parameters of the graded bandgap solar cell

Jsc(mA/cm2)	**Voc (V)**	**FF (%)**	**PCE (%)**
25,6101	1,05055	83,0614	22,3474

3.8 Influence of geometrical parameters

3.8.1 Effect of the absorber thickness

The simulation results of the variation of the absorber thickness are shown in the figures below. The graph illustrates how changing the perovskite absorber layer's thickness which ranges from 0.1 μm to 0.8 μm affects a number of photovoltaic cell performance measures.

The short-circuit current density (Jsc) rises with increasing layer thickness, reaching 28,2633 mA/cm² at 0.8 μm from 13,3914 mA/cm² at 0.1 μm. This suggests that larger layers are more efficient at producing charge carriers and absorbing light.

The open-circuit voltage (Voc) exhibits a marginal increase from 1,03351V to 1,06604V, indicating that the presence of a thicker layer could potentially mitigate recombination losses and thus lead to a modest increase in voltage.

The fill factor (FF) rises with thickness at first, peaking at 0.5 μm with 84,0089%, but when thickness goes beyond this point, it begins to decrease. This trend suggests that there is a maximum thickness for FF before resistive losses or enhanced recombination start to have detrimental impacts.

Finally, efficiency increases intensely from 11,2105% at 0.1 μm to a peak of 24,45% at 0.8 μm, matching the behaviour of Jsc.

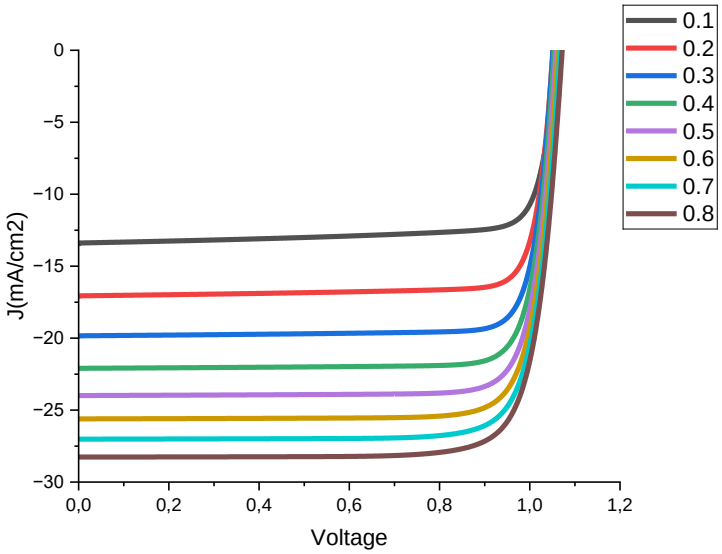

Figure 3.13 Effect of the thickness of the perovskite layer on the J(V) characteristic

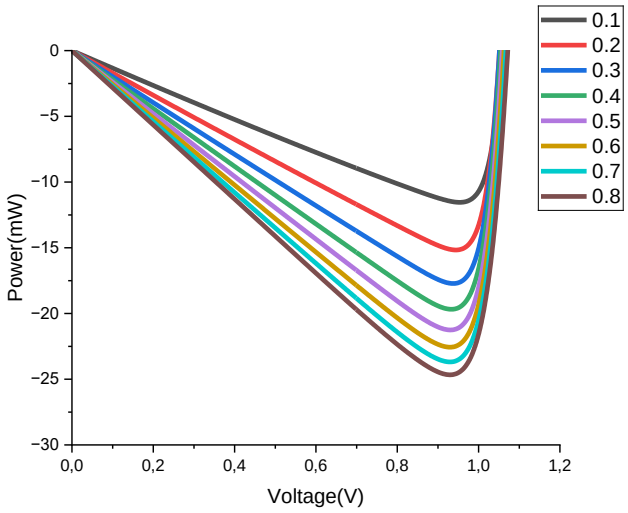

Figure 3.14 Effect of the perovskite layer doping on the P(V) characteristic

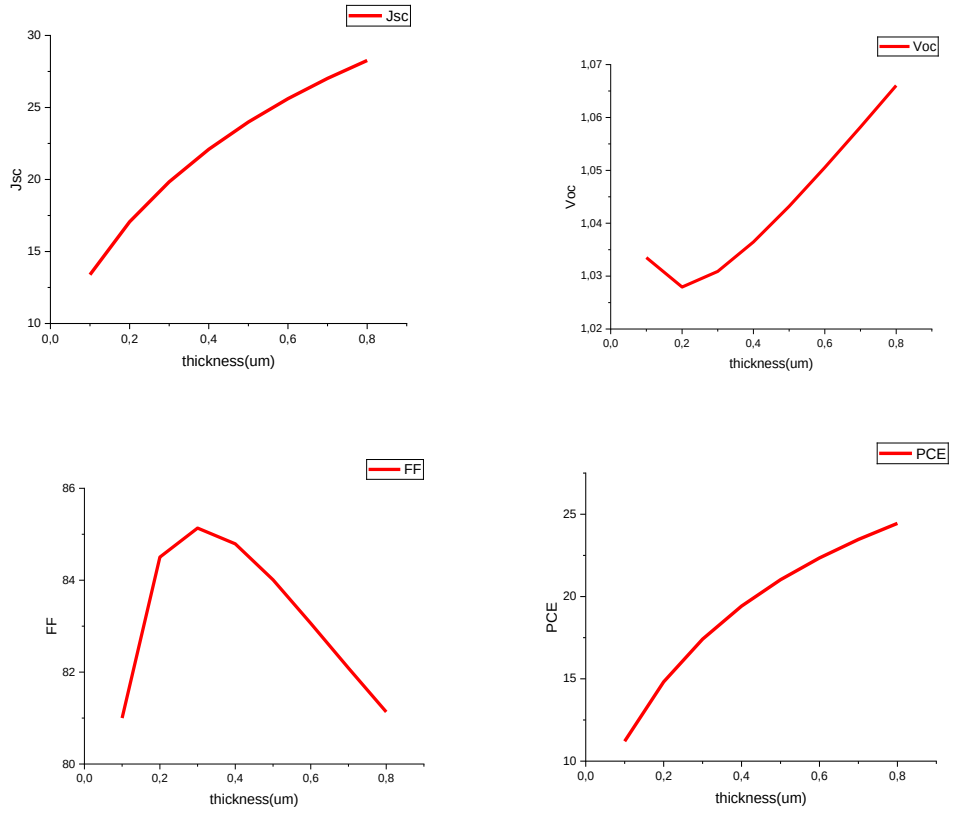

Figure 3.15 Photovoltaic parameters of the cell for different thickness values of the perovskite layer

Although Jsc and Voc are generally improved by larger perovskite layers, the decrease in FF above a certain thickness suggests a trade-off and raises the possibility that there is an ideal layer thickness that balances efficiency with other considerations like FF. The best efficiency seems to be achieved at or just over 0.6 µm, when absorption, charge production, and limited recombination are all balanced. All these parameters are presented in table 3.4.

Table 3.4 Photovoltaic parameters of the cell for different thickness values of the perovskite layer

Thickness (µm)	**Jsc(mA/cm2)**	**Voc (V)**	**FF (%)**	**PCE (%)**
0,1	13,3914	1,03351	80,9999	11,2105
0,2	17,0614	1,02794	84,5023	14,8201
0,3	19,8377	1,0309	85,1346	17,4106

0,4	22,0961	1,03646	84,7919	19,4188
0,5	23,9899	1,0432	84,0089	21,0243
0,6	25,6101	1,05055	83,0614	22,3474
0,7	27,0193	1,05818	82,089	23,4703
0,8	28,2633	1,06604	81,1346	24,4457

3.7.2 Effect of HTL thickness

The changing of the hole transport layer (HTL) thickness exhibits a minor downward trend for (Jsc) when the HTL thickness increases from 0.1 μm to 0.4 μm while the open-circuit voltage (Voc) remains constant.

Most significantly, there is a noticeable decrease in both the power conversion efficiency (PCE) and the fill factor (FF). Over the same thickness range, the PCE falls from 21.4573% to 21.1488%, while the fill factor falls from 86.0341% at 0.1 μm to 84.7981% at 0.4 μm. These trends suggest that although a thicker HTL may enhance (Voc) slightly, it negatively influences the cell's total efficiency, mostly through negative effects on Jsc and FF. This indicates that by maintaining higher Jsc and FF values, an ideally thinner HTL may improve cell performance and maximize overall efficiency. Table 3.5 displays[L1] the values of the photovoltaic performances for different HTL thicknesses layer.

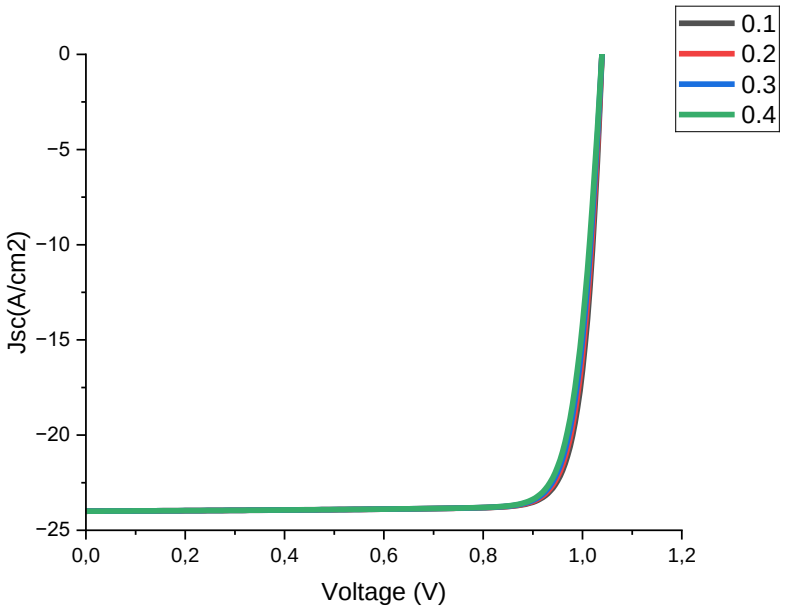

Figure 3.16 Effect of thickness of the HTL layer on the J(V) characteristic

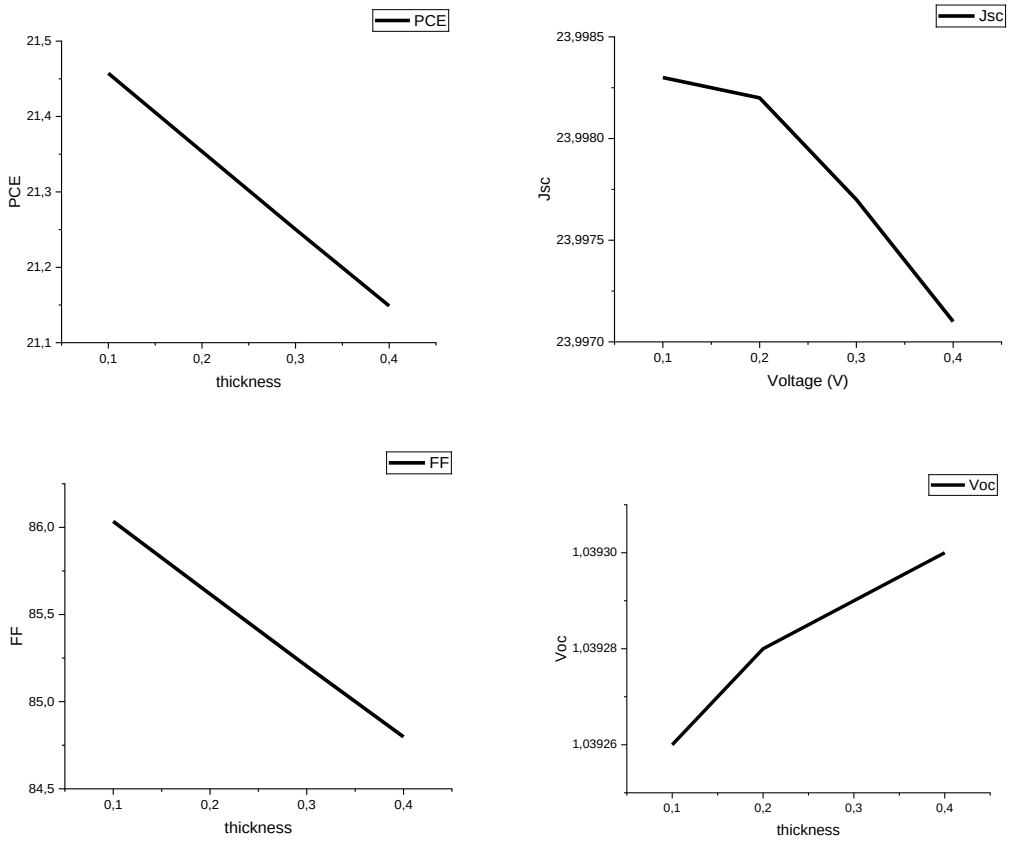

Figure 3.17: Photovoltaic parameters of the cell for different thickness values of the HTL layer

Table 3.5 Photovoltaic parameters of the cell for different thickness values of the HTL layer

Thickness (µm)	Jsc (mA/cm2)	Voc (V)	FF (%)	PCE (%)
0,1	23,9983	1,03926	86,0341	21,4573
0,2	23,9982	1,03928	85,6174	21,3537
0,3	23,9977	1,03929	85,2037	21,2503
0,4	23,9971	1,0393	84,7981	21,1488

3.8.3 Effect of ETL thickness

The effect of changing the electron transport layer (ETL) thickness is presented in the following graphs. The short-circuit current density (Jsc) and the open-circuit voltage (Voc) remain constant at 23.9983 mA/cm² and 1.03926 V respectively, across four distinct thicknesses (0.1, 0.2, 0.3, and 0.4 µm). Nonetheless suggesting that variations in the ETL thickness do not significantly affect these parameters, as the ETL thickness grows, there is a small but steady decline in the fill factor (FF). The efficiency of the cell may be slightly decreased by thicker ETL layers, according to this minor fall. This shows that the ideal ETL thickness is one that maximizes efficiency without significantly altering other electrical parameters.

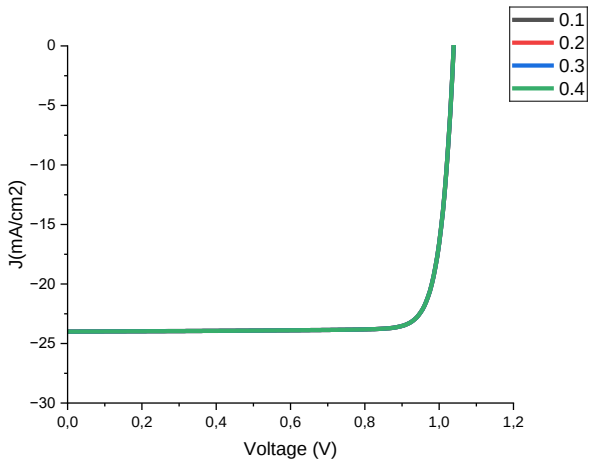

Figure 3.18 Effect of thickness of the ETL layer on the J(V) characteristic

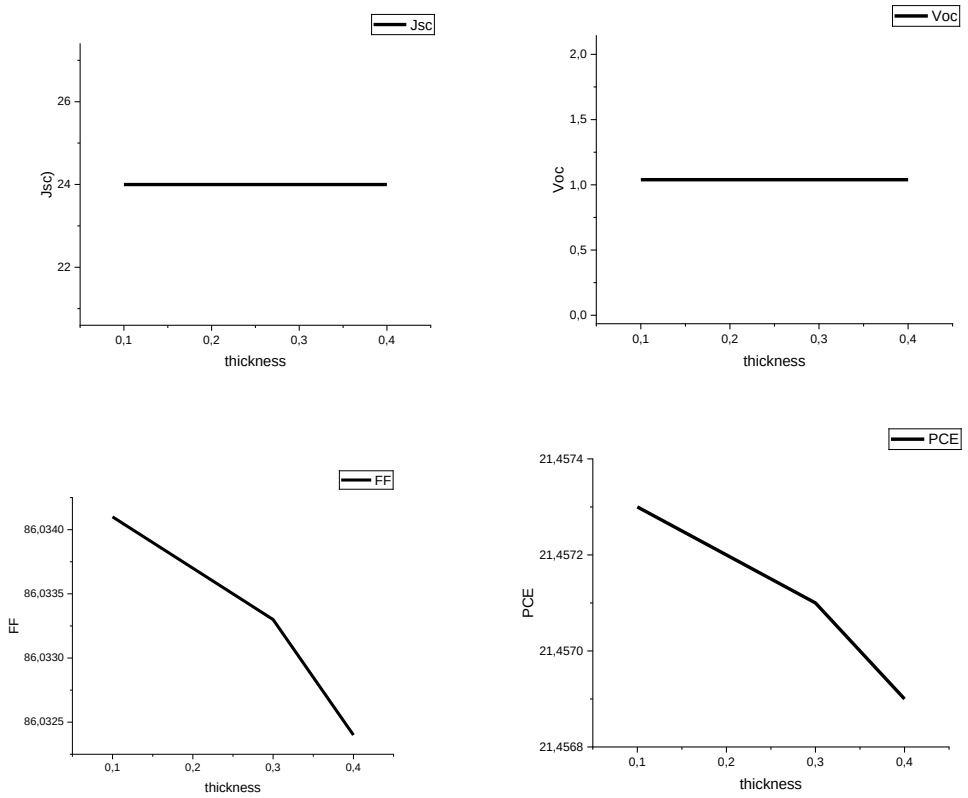

Figure 3.19: Photovoltaic parameters of the cell for different thickness values of the ETL layer

Table 3.6: Photovoltaic parameters of the cell for different thickness values of the ETL layer

Thickness (µm)	Jsc (mA/m2)	Voc (V)	FF (%)	PCE (%)
0,1	23,998	1,03926	86,0341	21,4573
0,2	23,9983	1,03926	86,0337	21,4572
0,3	23,9983	1,03926	86,0333	21,4571
0,4	23,9983	1,03926	86,0324	21,4569

3.9 Influence of doping concentration

3.9.1 Effect of ETL doping

The dataset shows how different doping concentrations in the electron transport layer (ETL) affect a solar cell's performance parameters. The range of doping levels that were investigated was $1x10^{17}$–$1x10^{20}$ atoms/cm³. According to the findings, the short-circuit current

density (Jsc) drops rapidly when the doping level rises above $1x10^{18}$, from 23.9982 mA/cm² to 20.5312 mA/cm² at $1x10^{20}$. However, at lower doping concentrations, Jsc remains rather steady.

This implies that greater doping concentrations might promote recombination processes, hence reducing the effective charge separation required for increased current output. Additionally, when the doping level increases, the open-circuit voltage (Voc) gradually drops from 1.05817 V at the lowest to 1.02391 V at the highest. Similarly, as the doping concentration rises, the fill factor (FF) falls from 83.3239% to 81.3068%. A notable pattern can be seen in power conversion efficiency (PCE), which peaked at 21.3537% with 1e18 doping and then decreased to 17.0924 % with $1x10^{20}$.

A moderate amount of doping can improve performance, but excessive doping can negatively influence the overall efficiency of the solar cell. This decrease in efficiency at greater doping levels highlights the cumulative negative impacts on Jsc, Voc, and FF. To balance the advantages of enhanced charge transfer against the disadvantages of higher recombination and electrical resistance.

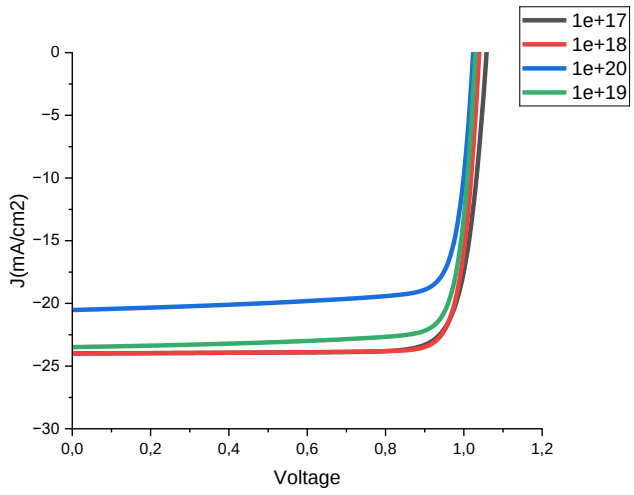

Figure 3.20 Effect of doping of the ETL layer on the J(V) characteristic

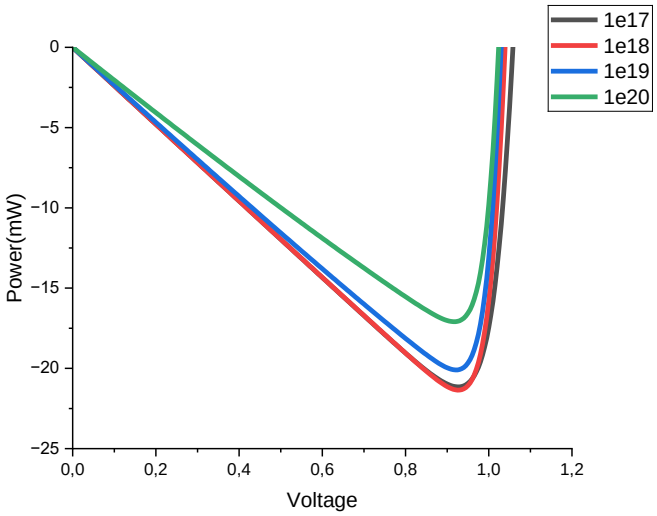

Figure 3.21 Effect of doping of the ETL layer on the P(V) characteristic

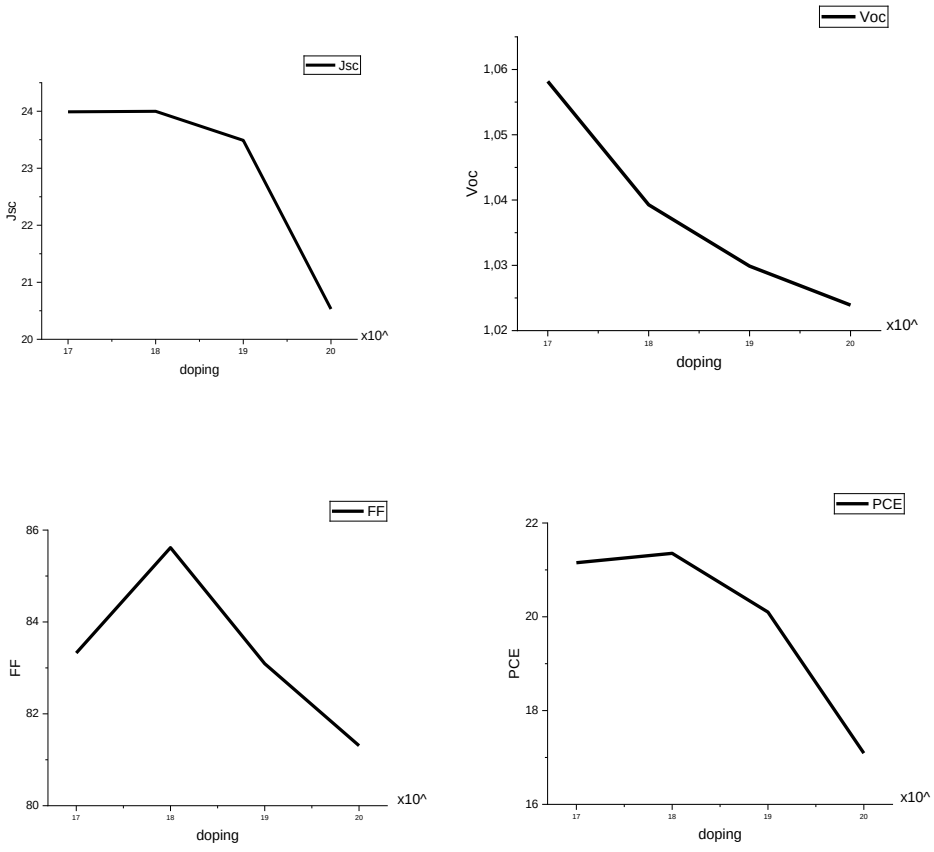

Figure 3.22: Photovoltaic parameters of the cell for different doping values of the ETL layer

Table 3.7: Photovoltaic parameters of the cell for different doping values of the ETL layer

Doping (cm^{-3})	**Jsc (mA/cm2)**	**Voc (V)**	**FF (%)**	**PCE%**
$1x10^{17}$	23,9898	1,05817	83,3239	21,152
$1x\ 10^{18}$	23,9982	1,03928	85,6174	21,3537
$1x\ 10^{19}$	23,4887	1,02988	83,0916	20,1003
$1x\ 10^{20}$	20,5312	1,02391	81,3068	17,0924

3.9.2 Effect of HTL doping

Different doping concentrations in a solar cell's hole transport layer (HTL) affect important performance indicators. Each parameter shows significant variations as doping concentrations rise from 1e17 to 1e20 atoms/cm^3.

As doping levels increase, the fill factor (FF) gradually drops from 83.3239% to 79.9957%, suggesting a possible increase in internal resistance or less effective charge collection. As with FF and the short-circuit current density (Jsc), power conversion efficiency (PCE) likewise decreases, going from 21.152% at the lowest doping level to 20.2131% at the highest.

The short circuit current (Jsc) itself drops from 23.9898 mA/cm^3 to 23.1309 mA/cm^3, indicating that increased doping concentrations could intensify recombination processes and have an adverse effect on the generation that is now occurring.

On the other hand, there is a rise in the open-circuit voltage (Voc), which increases from 1.05817 V at $1x10^{17}$ to 1.09238 V at $1x10^{20}$. Better hole extraction and less charge recombination at the anode, which are advantageous for reaching higher voltages, may be the cause of this. Even while increasing doping has a beneficial effect on Voc, the overall effect on the HTL shows a net disadvantage, especially since the gains in voltage are not enough to make up for the losses in fill factor and current.

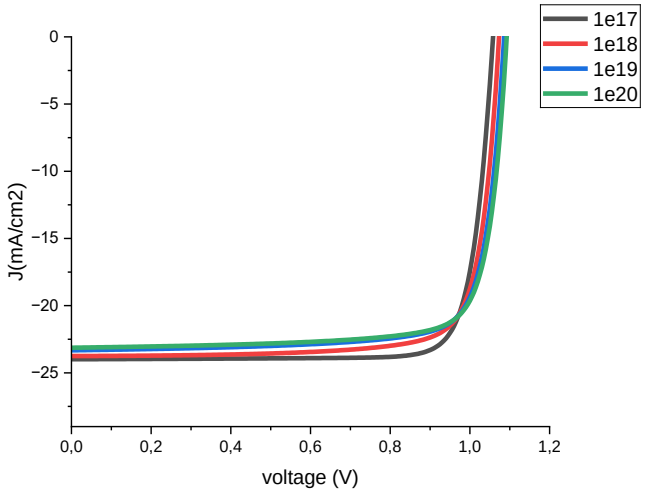

Figure 3.23 Effect of doping of the HTL layer on the J(V) characteristic

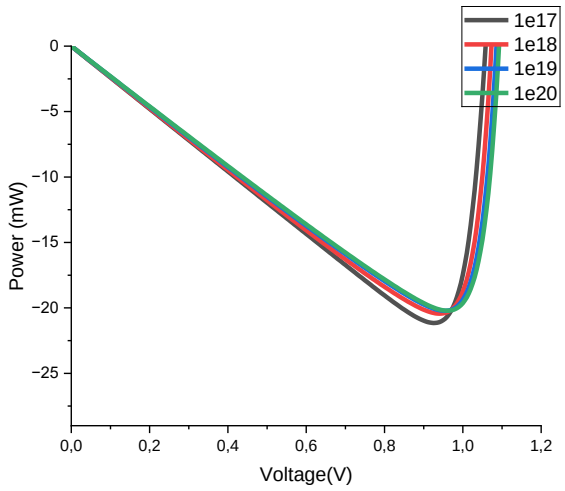

Figure 3.24: Effect of doping of the HTL layer on the P(V) characteristic

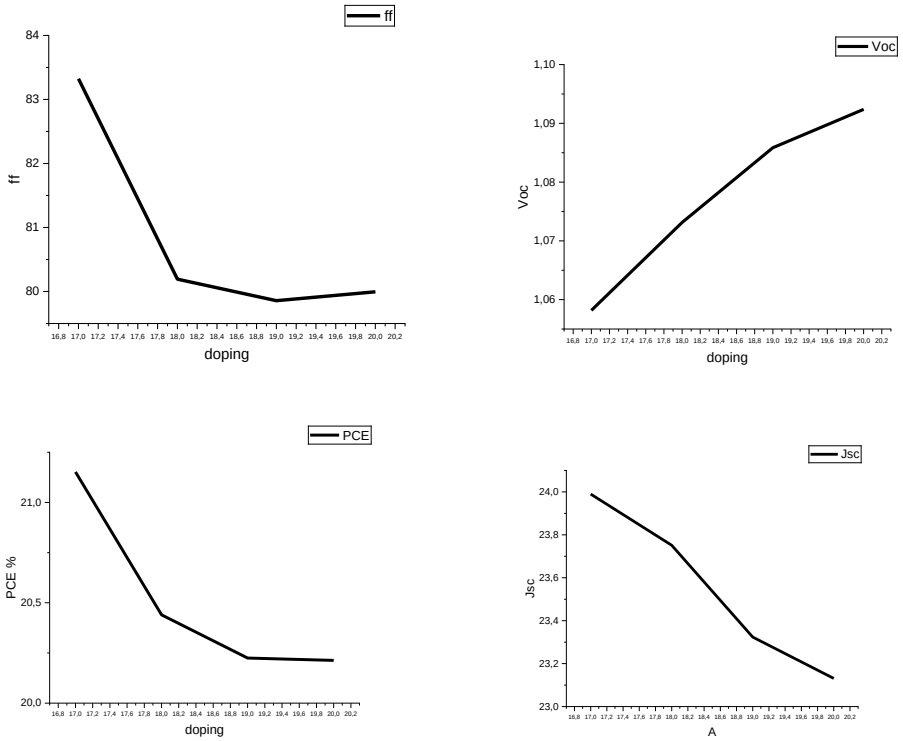

Figure 3.25: Photovoltaic parameters of the cell for different doping values of the HTL layer

Table 3.8 Photovoltaic parameters of the cell for different doping values of the HTL layer

Doping (cm^{-3})	**FF(%)**	**PCE%**	**Voc (V)**	**Jsc (mA/cm2)**
$1x10^{17}$	83,3239	21,152	1,05817	23,9898
$1x10^{18}$	80,1928	20,4399	1,07313	23,7515
$1x10^{19}$	79,8565	20,2245	1,08585	23,3237
$1x10^{20}$	79,9957	20,2131	1,09238	23,1309

3.10 Simulation of the optimal perovskite

The best arrangements for the different layers in solar cells can be summed up as follows: Increasing the thickness of the absorber layer in the graded solar cell to 0.8 μm resulted in a steady improvement in efficiency, with a peak efficiency of 24.63%. According to this, thicker absorber layers are thought to be more efficient in absorbing light and turning it into electricity, however because of the decreasing fill factor (FF), 0.6 μm is the ideal thickness, with a PCE of 22.34%.

The Hole Transport Layer (HTL) and Electron Transport Layer (ETL) showed greater efficiency with a minimum thickness of around 0.1 μm. Additionally, the lowest doping level measured (1e17) yielded the highest efficiency in both the HTL and ETL layers, indicating that lower doping levels would be beneficial for these layers. Therefore, employing a absorber layer at 0.6 μm while keeping thinner and lower-doped HTL and ETL layers would be the best strategy for solar cell construction using this data in order to increase overall solar cell efficiency.

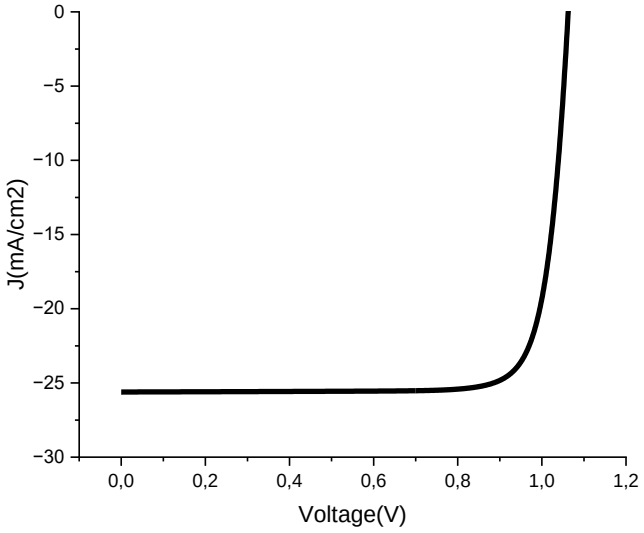

Figure 3.26 J-V characteristic of optimal graded perovskite (MAPbI3) solar cell

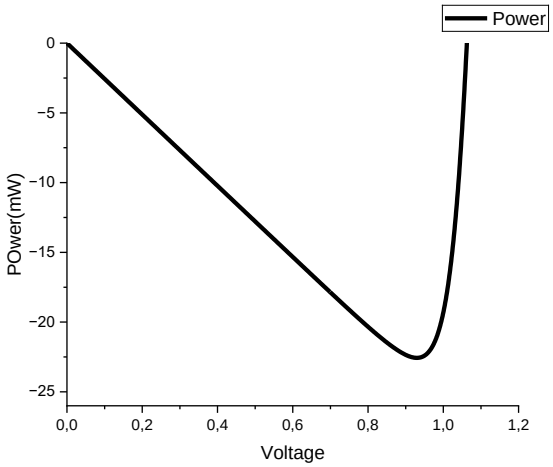

Figure 3.27 P-V characteristic of optimal graded perovskite (MAPbI3) solar cell

Table 3.9: Photovoltaic parameters of optimal graded bandgap solar cell

Voc (V)	**Jsc (mA/cm2)**	**FF (%)**	**PCE%**
1,05055	25,6101	83,0614	22,3474

3.11 Conclusion

We have thoroughly examined the Silvaco Tcad simulator's numerical simulation and performance analysis of a perovskite solar cell in this chapter. The construction of the solar cell, including its optical properties and geometric and physical parameters, was the subject of our inquiry. The evaluation of the photovoltaic performances involved a thorough analysis of the J(V) and P(V) characteristics, as well as important photovoltaic parameters such as fill factor (FF), open-circuit voltage (Voc), short-circuit current density (Jsc), and overall efficiency (PCE).

We also investigated the possibility of improving solar cell performance by introducing a graded energy bandgap by replacing bromine with iodine. The spectral response was not affected by the bandgap changes as predicted. This surprising outcome raises the possibility that additional variables are influencing photovoltaic behavior, which calls for more research on the relationship between material characteristics and device performance.

The effects of different doping concentrations within these layers, as well as the thickness of the absorber, hole transport layer (HTL), and electron transport layer (ETL), were also examined in this chapter. Every adjustment was carefully examined to determine how it affected the photovoltaic performance, which revealed particular circumstances in which the efficiency of the solar cell might be optimized. Finally, our simulations highlight how important it is to precisely optimize parameters in order to maximize the performance and efficiency of perovskite solar cells. These results open up new avenues for future research focused at improving and achieving high-performance photovoltaic devices, in addition to contributing to the current state of solar cell technology development. The thorough study's insights stimulate greater research into material and structural advancements that may lead to more effective and sustainable solar energy solutions.

General Conclusion

Numerous studies have been conducted on the potential of graded bandgap perovskite MAPb(I1-x-Brx)2 solar cells, demonstrating notable advances in photovoltaic technology. Through numerical simulations with the Silvaco Tcad simulator, one may significantly improve photovoltaic metrics like as fill factor (FF), open-circuit voltage (Voc), short-circuit current (Jsc), and overall efficiency (η) by fine-tuning the bandgap in perovskite structures.

The study shows that performance can be greatly enhanced by varying the bandgap and the optical and physical properties of the solar cell layers. By maximizing absorption across the solar spectrum, the graded energy bandgap increases the efficiency of solar energy conversion.

The research also sheds light on the impacts of doping concentration and layer thickness, highlighting the necessity of a balanced approach to solar cell design. A peak efficiency of 22,35% was obtained by increasing the thickness of the absorber layer to 0.6 μm, which suggests improved light capture and power conversion. About 0.1 μm was the ideal thickness for the Electron Transport Layer (ETL) made of compact titanium oxide (C-TiO2) and the Hole Transport Layer (HTL) made of Spiro-OMeTAD. For both layers, the lowest doping level (1e17) produced the highest efficiencies. To optimize efficiency, it is therefore ideal to combine thinner and lower-doped HTL and ETL layers with a thicker absorber layer (0.6 μm).

The study emphasizes how graded bandgap perovskites have the ability to completely transform the photovoltaics market, offering an efficient and cost-effective future for renewable energy solutions. This study not only broadens our knowledge of perovskite materials but also has important ramifications for the production of solar cells for the commercial market, which could lead to a rise in the use of solar energy.

BIBLIOGRAPHY

[1]: Noemi Guerra, César Palacios Arias , Felice Crupi , Marco Guevara Operation and physics of photovoltaic solar cells: an overview, 2018

[2] : Tiantian Zhang,Ruzhu Wang, in Handbook of Energy Efficiency in Buildings, High Efficiency Plants and Building Integrated Renewable Energy Systems, 2019

[3]: https://www.pveducation.org/pvcdrom/solar-cell-operation

[4]: Vincenzo Franzitta, Aldo Orioli , and Alessandra Di Gangi, Assessment of the Usability and Accuracy of the Simplified One-Diode Models for Photovoltaic Modules, 2016

[5] Arno HM Smets ,Klaus Jäger ,Olindo Isabella ,René ACMM van Swaaij Miro Zeman : Solar energy The physics and engineering of photovoltaic conversion, technologies and systems, 2016

[6]Sandeep Prabhu M, Archana Balyan,Gangadhara, Pooja Singh, P-V and I-V Characteristics of Solar Cell, 2021

[7] Victoria Gonzalez-Pedro ,Emilio J. Juarez-Perez,Waode-Sukmawati Arsyad,Eva M. Barea,Francisco Fabregat-Santiago,Ivan Mora-Sero*and,Juan Bisquert, : General Working Principles of CH3NH3PbX3 Perovskite Solar Cells, 2014

[8] :J. Lakshmi Prasanna Pranay Ranjan d a , Ekta Goel , Atul Kumar, Bandgap graded perovskite solar cell for above 30% efficiency, 2022

[9] : Ashwith Kumar Chilvery, Ashok K Batra, Bin Yang, Kai Xiao, Padmaja Guggilla, Mohan D Aggarwal, Raja Surabhi, Ravi B Lal, James R Currie, and Benjamin G Penn. Perovskites: transforming photovoltaics, a mini review. Journal of Photonics for Energy, 2015.

[10] : Laxmi Nakka, Yuanhang Cheng, Armin Gerhard Aberle, and Fen Lin, Analytical Review of Spiro-OMeTAD Hole Transport Materials: Paths Toward Stable and Efficient Perovskite Solar Cells, 2022

[11] : Fedwa El Mellouhi, El Tayeb Bentria, Sabre Kais, Fahhad Alharbi, sergey N Rashkeev, Enhancing Intrinsic Stability of Hybrid Perovskite Solar Cell by Strong, yet Balanced, Electronic Coupling , 2016

BIBLIOGRAPHY

[12] : Nam-Gyu Park, Perovskite solar cells: an emerging photovoltaic technology, 2014

[13] : Sagar Bhattaraia,e , Rahul Pandeyb, Jaya Madanb, Firdausa Ahmedc, Shahnaz Shabnamd, Performance improvement approach of all inorganic perovskite solar cell with numerical simulation, 2022

[14] : Rabia Sharif, Arshi Khalid,b Syed Waqas Ahmad,a Abdul Rehman, Haji Ghulam Qutab,a Hafiz Husnain Akhtar,a Khalid Mahmood, aShabana Afzalc and Faisal Saleem, A comprehensive review of the current progresses and material advances in perovskite solar cells, 2023

[15] : Juvet Nche Fru1, Nolwazi Nombona and Mmantsae Diale, Characterization of Thin MAPb($I_{1-x}Br_x$)$_3$ Alloy Halide Perovskite Films Prepared by Sequential Physical Vapor Deposition, 2021

[16] : Fengren Cao, Meng Wang LiangLi, Graded energy band engineering for efficient perovskite solar cells , 2020

[17] : Dariush Madadi, Achieving beyond 26.6% efficiency for graded bandgap perovskite solar cell: Theoretical study, 2023

[18] :Vidhya Selvanathan, Comprehensive Guide on Organic and Inorganic Solar Cells, Md. Akhtaruzzaman, 2022

[19] :Fan Fu, Stefano Pisoni, Thomas P. Weiss, Thomas Feurer, Aneliia Wäckerlin, Peter Fuchs, Shiro Nishiwaki, Lukas Zortea, Ayodhya N. Tiwari, and Stephan Buecheler, Compositionally Graded Absorber for Efficient and Stable Near-Infrared-Transparent Perovskite Solar Cells, 2018

[20] : Sneha A. Kulkarni, Tom Baikie,a Pablo P. Boix, Natalia Yantara,Nripan Mathews, and Subodh Mhaisalkar, Band-gap tuning of lead halide perovskites using a sequential deposition process,2014

[21] : Ashwith Kumar Chilvery Ashok K. Batra Bin Yang Kai Xiao Padmaja Guggilla Mohan D. Aggarwal Raja Surabhi Ravi B. Lal James R. Currie Benjamin G. Penn, Perovskites: transforming photovoltaics, a mini-review, 2015

[22] : https://us.solarpanelsnetwork.com/blog/solar-panel-spectral-response

[23] : Samy Almosni, Ludmila Cojocaru, Debin Li, Satoshi Uchida,Takaya Kubo, Hiroshi Segawa, Tunneling-Assisted Trapping as one of the PossibleMechanisms for the Origin of Hysteresis in PerovskiteSolar Cells

[24] :Fan Fu, Stefano Pisoni, Thomas P. Weiss, Thomas Feurer, Aneliia Wäckerlin,Peter Fuchs, Shiro Nishiwaki, Lukas Zortea, Ayodhya N. Tiwari, and Stephan Buecheler, Compositionally Graded Absorber for Efficient and StableNear-Infrared-Transparent Perovskite Solar Cells

[25] : Atlas User's Manual book